## TITLE PAGE

**Title**: Divergent opioid-mediated suppression of inhibition between hippocampus and neocortex across species and development

**Authors**: Adam P. Caccavano[1*], Sarah Kimmel[1], Anna Vlachos[1], Vivek Mahadevan[1], June Hoan Kim[1], Geoffrey Vargish[1], Ramesh Chittajallu[1], Edra London[1], Xiaoqing Yuan[1], Steven Hunt[1], Mark A. G. Eldridge[2], Alex C. Cummins[2], Brendan E. Hines[2], Anya Plotnikova[2], Arya Mohanty[2], Bruno B. Averbeck[2], Kareem Zaghloul[3], Jordane Dimidschstein[4], Gord Fishell[4,5], Kenneth A. Pelkey[1*] and Chris J. McBain[1*]

**Affiliations:**

[1]Section on Cellular and Synaptic Physiology, *Eunice Kennedy Shriver* National Institute of Child Health and Human Development (NICHD), National Institutes of Health (NIH), Bethesda, MD, USA

[2]National Institute of Mental Health (NIMH), NIH, Bethesda, MD, USA

[3]National Institute of Neurological Disorders and Stroke (NINDS) Intramural Research Program, NIH Bethesda, MD, USA

[4]Stanley Center for Psychiatric Research, Broad Institute of Harvard and MIT, Cambridge, MA, USA

[5]Department of Neurobiology, Harvard Medical School, Boston, MA, USA

**Corresponding Authors Email**: adam.caccavano@nih.gov (APC), pelkeyk2@nih.gov (KAP), mcbainc@nih.gov (CJM)

**Lead Contact**: adam.caccavano@nih.gov

## SUMMARY

Opioid receptors within the CNS regulate pain sensation and mood and are key targets for drugs of abuse. Within the adult rodent hippocampus (HPC), μ-opioid receptor agonists suppress inhibitory parvalbumin-expressing interneurons (PV-INs), thus disinhibiting the circuit. However, it is uncertain if this disinhibitory motif is conserved in other cortical regions, species, or across development. We observed that PV-IN mediated inhibition is robustly suppressed by opioids in HPC but not neocortex in mice and nonhuman primates, with spontaneous inhibitory tone in resected human tissue also following a consistent dichotomy. This hippocampal disinhibitory motif was established in early development when immature PV-INs and opioids already influence primordial network rhythmogenesis. Acute opioid-mediated modulation was partially occluded with morphine pretreatment, with implications for the effects of opioids on hippocampal network activity during circuit maturation as well as learning and memory. Together, these findings demonstrate that PV-INs exhibit a divergence in opioid sensitivity across brain regions that is remarkably conserved across evolution and highlights the underappreciated role of opioids acting through immature PV-INs in shaping hippocampal development.

## INTRODUCTION

The endogenous opioid system in the central nervous system (CNS) plays a crucial role in pain sensation, stress response, and mood[1,2]. Opioid receptors are also key targets for exogenous drugs of abuse including heroin and fentanyl. With a high risk of dependency, mortality from respiratory depression, and epidemic levels of abuse, opioids have fueled a public health emergency within the US, resulting in over 80,000 fatalities in 2021[3] and an estimated economic burden of over a $1 trillion annually[4]. One third of pregnant women report opioid use, and in almost 60,000 annual pregnancies there is reported opioid abuse[5]. Children born to opioid-dependent mothers are at increased risk of neurodevelopmental deficits within cognitive, psychomotor, and language domains[6]. Despite these risks, there remains an urgent need for potent and safe analgesics. To develop improved opioid or non-opioid analgesics, research is required into the mechanisms of opioids at the cellular and microcircuit level. Novel genetic tools enable us to study the mechanisms of opioids in distinct neuronal subpopulations across species, with the eventual goal of creating more targeted treatments and elucidating endogenous opioid function.

Endogenous opioids (e.g., endorphins, enkephalins) and exogenous opiates (e.g., morphine, fentanyl) act with differing specificities on mu, delta, and kappa opioid receptors (μOR, δOR, and κOR). Notably, μORs are associated with reward-processing of both natural stimuli and drugs of abuse[1,7,8]. These $G_i/G_o$ coupled metabotropic receptors have both pre- and post-synaptic inhibitory secondary effects[9,10]: the pre-synaptic closure of $Ca^{2+}$ channels[11,12], the post-synaptic opening of inward-rectifying $K^+$ channels[13-15], and the modulation of HCN channels, which mediate the non-specific cation current $I_h$[13,16,17]. Within the hippocampus (HPC), μOR activation has an overall disinhibitory effect on the network[18-21] due to a preferential suppression of the inhibitory GABAergic cell population[22-24]. Within the CA1 region of HPC, this suppression of inhibition has been primarily associated with parvalbumin-expressing interneurons (PV-INs)[25-27]. Perisomatic-targeting PV-INs of the HPC highly express μORs/δORs, though not exclusively, as lower percentages of dendritic-targeting somatostatin-expressing interneurons (SST-INs) and neuropeptide Y-expressing ivy and neurogliaform cells (NPY-INs) also express these receptors[28,29]. As with hippocampal PV-INs, opioids can suppress both hippocampal SST-INs[30] and NPY-INs[31]. Although μORs/δORs are expressed throughout the CNS[32-36], most functional cellular studies of opioid suppression of inhibition have been restricted to the adult rodent HPC, with fewer studies focusing on other cortical regions, species, or across development.

Hippocampal and neocortical PV-INs are critical organizers of rhythmic activity important for learning and memory including sharp wave ripples (SWRs) and gamma oscillations[37]. PV-INs throughout the forebrain have common developmental origins in the medial ganglionic eminence (MGE)[38] and are often treated as monolithic with common circuit motif functionality, leading to textbook observations of neuromodulatory control of inhibitory microcircuits that may not generalize across brain regions[39]. PV-

INs within different brain regions may express unique receptors, as is the case in striatum, where PV-INs express the $CB_1$ cannabinoid receptor[40], which in the hippocampus is selectively expressed by cholecystokinin-expressing interneurons (CCK-INs)[41]. Given the degree of inhibitory control this neuronal population has over cortical microcircuits, any regional specializations become essential to understand if PV-INs are expected to participate in or be targets of therapeutic interventions for addiction. Moreover, it is essential to translate any rodent findings to higher species as cellular and circuit motifs may have diverged over 70 million years of evolution, particularly in light of recent evidence of human-specific innovations in channel expression and electrophysiological properties of PV-INs[42,43].

In the present study we examined the opioid-mediated suppression of PV-INs across cortical regions, species, and development. We discovered this disinhibitory motif is unique to the hippocampus. In contrast to hippocampal PV-INs, neocortical PV-INs were less colocalized with μORs, less hyperpolarized by μOR agonists, and optogenetically-evoked PV-IN output was unaffected by μOR selective drugs. By employing a viral strategy with the evolutionally conserved and PV-specific E2 enhancer of the voltage-gated sodium channel *Scn1a*[44], we determined this regional divergence translated to virally transfected nonhuman primates (NHPs), as well as spontaneous inhibitory currents in resected human tissue. Moreover, this hippocampal disinhibitory motif was observed in early postnatal development, just as synapses were being established, with important control over spontaneous activity of the developing hippocampus including giant depolarizing potentials (GDPs). Finally, we observed this acute opioid-mediated suppression of inhibition in the hippocampus to be partially occluded in adult mice pre-treated with morphine. The hippocampal specificity of the opioid-mediated disinhibition has profound implications for rhythmic activities supporting learning and memory. Indeed, prior studies have demonstrated that both SWRs[45] and gamma oscillations[46] are highly sensitive to opioid administration. In the present study we extend these findings to opioid modulation of GDPs, with severe implications for the harmful aspects of opioid use *in utero* and in early development. Together, our findings demonstrate that despite common developmental origins in the MGE, not all PV-INs are destined to fulfill identical circuit roles. Their response to opioids is highly dependent on cortical region, is established in early development, and is remarkably conserved across mammalian species.

## RESULTS

### *μORs are enriched in and selectively hyperpolarize hippocampal PV-INs.*

μORs are expressed throughout hippocampus and neocortex[1], and within the hippocampus are highly enriched in PV-INs[28,29]. However, less is known about the specificity of μOR expression to PV-INs throughout neocortex. To address this, we quantified via immunohistochemistry (IHC) PV-μOR colocalization by staining for PV in μOR-mCherry mice (Fig. 1A-B). We observed an increased correlation between PV and μOR in synaptic processes of CA1 *stratum pyramidale* (*str. pyr.*) as compared to neocortical pyramidal cell layers (both supragranular layers 2/3 and infragranular layers 5/6) in primary motor (M1), somatosensory (S1) and visual (V1) cortex (Fig. 1B, D). No differences were observed in the overall intensity of PV or μOR between these four regions (Fig. 1D, colored traces). We next assessed the levels of mRNA via *in situ* hybridization (ISH) RNAscope, observing a decreased percentage of *Pvalb*+ somata colocalized with *Oprm1* (encoding μORs) in M1, S1, and V1 relative to CA1 (Fig. 1C, E). Finally, to assess if mRNA associated with the translational machinery was altered, we employed a RiboTag sequencing approach of MGE-derived interneurons (of which PV-INs comprise a substantial fraction[47]) employing Nkx2.1$^{Cre/+}$:Rpl22(RiboTag)$^{HA/HA}$ mice[48-50]. We observed a selective enrichment of *Oprm1* in hippocampal MGE-INs relative to neocortical MGE-INs and all bulk hippocampal/neocortical tissue (Fig. 1F).

μORs hyperpolarize neurons and reduce neurotransmitter release via combined interactions with inward-rectifying $K^+$ channels and closure of presynaptic $Ca^{2+}$ channels[9,10]. To determine whether a functional divergence existed between hippocampal and neocortical PV-INs, we recorded in a whole-cell configuration currents elicited by the administration of μOR agonist DAMGO (100 nM) and antagonist CTAP (500 nM) (Fig. 1G) in PV-tdTomato$^{+/-}$ mice (Fig. 1H). Consistent with prior studies[25,26], we observed an outward hyperpolarizing current from DAMGO administration in CA1 *str. pyr.* PV-INs voltage-clamped to -50 mV (60 ± 19 pA, Fig. 1I, $J_1$-$L_1$). However, no significant change in holding current was observed in V1 PV-INs (12 ± 18 pA, Fig. 1I, $J_2$-$L_2$). Of the CA1 PV-INs with sufficiently recovered morphology to assess axonal target ($n_{cell}$ = 8 of 11), 75% were perisomatic-targeting (6 of 8), while 25% (2 of 8) exhibited bistratified morphology targeting apical and basal dendrites. Notably, both bistratified cells exhibited a hyperpolarizing DAMGO-elicited current. All V1 PV-INs with sufficiently labeled axons ($n_{cell}$ = 11 of 15) were perisomatic-targeting with somata spanning cortical layers 2 through 6. In CA1 PV-INs, there was also an observed decrease in input resistance (Fig. 1$M_1$), consistent with the opening of ion channels, which was not observed in V1 PV-INs (Fig. 1$M_2$). Together, these findings point to a transcriptional, translational, and functional enrichment of μORs within hippocampal versus neocortical PV-INs.

***Opioids selectively suppress hippocampal but not neocortical PV-IN mediated inhibition.***

To determine if the selective enrichment of μORs within hippocampal PV-INs can reduce inhibitory synaptic transmission, we adopted an optogenetic approach to light-activate PV-INs and record their output in downstream pyramidal cells (PCs) in $PV^{Cre/+}$:$ChR2^{fl/+}$ mice (Fig. 2A-B). $GABA_A$-mediated currents were pharmacologically isolated with bath administration of AMPA, NMDA, and $GABA_B$ antagonists (μM: 10 DNQX, 50 DL-APV, and 1 CGP55845 respectively), with drugs of interest (nM: 100 DAMGO, 500 CTAP) bath administered for at least 5 minutes. Consistent with prior hippocampal studies[25,26], light-evoked inhibitory post-synaptic currents (leIPSCs) were suppressed by DAMGO in CA1-PCs (Fig. 2C). To assess a pre- or post-synaptic mechanism, we analyzed the coefficient of variation (Fig. 2C), and in a subset of cells, the paired pulse ratio (Fig. 2D), observing an increase in both metrics (Fig. 2E-F), pointing to a presynaptic mechanism and consistent with prior studies[25,27]. Notably however, PV-IN output was differentially modulated between HPC and CTX, with significant suppression (64 ± 5% of baseline) observed in CA1-PCs and no suppression (108 ± 6% of baseline) observed in M1-PCs (Fig. 2G). To broadly assess this across cortical regions, we recorded leIPSCs in three hippocampal (CA1, CA3, dentate gyrus DG) and three neocortical regions (M1, S1, V1). Additionally, as differences in PV connectivity have been reported between superficial (closer to *str. rad.*) and deep (closer to *str. or.*) PCs (sPCs and dPCs respectively)[51,52], we segregated recordings from these cell populations. Both in CA1-sPCs (Fig. 2H) and CA1-dPCs (Fig. 2I), leIPSCs were suppressed by DAMGO, with no observed difference in the baseline normalized response between these cell populations ($p = 0.1351$, Fig. S2A). Both in CA1-sPC and CA1-dPC recordings, CTAP reversed the DAMGO-mediated suppression, although this could also be achieved through wash alone (data not shown). leIPSCs recorded in CA3-PCs were also suppressed by DAMGO, although this did not fully reverse with either administration of CTAP or wash (Fig. 2J). Interestingly, this long-lasting μOR-mediated suppression in CA3 is similar to observations of a long-lasting δOR-mediated suppression within CA2 that was not observed in CA1[53]. In DG granule cells (DG-GCs), we observed a highly variable response, with no significant group effect of either DAMGO or CTAP (Fig. 2K). Throughout neocortex, we also observed highly variable responses with no significant group effects of either DAMGO or CTAP in M1 (Fig. 2L), S1 (Fig. 2M), and V1 (Fig. 2N). Neocortical PCs were recorded in both supragranular (2/3) and infragranular (5/6) layers. To address the possibility that differing opioid sensitivity between cortical layers could be contributing to the increased variance in the observed leIPSC amplitude, we combined M1, S1, and V1 PCs and segregated the combined data across L2/3 and L5/6, with no differences observed in the baseline normalized DAMGO response ($p = 0.2913$, Fig. S2B).

We next examined the role of sex in our data, as there have been reported sex differences in analgesic response, with morphine less potent in women[54]. Pertinent to our study, there are reported sex differences in the trafficking of μORs in hippocampal PV-INs[55,56]. Most regions we assessed were not

sufficiently powered to segregate along sex. However, by combining all CA-PCs (CA1-sPCs, CA1-dPCs, CA3-PCs) and all CTX-PCs (M1, S1, V1), we achieved sufficiently powered groups to analyze via 2-way ANOVA the effects of sex and region. A significant effect of region was found ($p < 0.0001$) with sex not reaching significance ($p = 0.2059$). Fisher's *post hoc* comparisons yielded significant regional differences in males and females, but no significant sex differences in CA or CTX (Fig. S2C). Thus, although there could be minor differences driving an almost significant sex effect in CTX (Fig. S2C), it did not appear to be a driving confounder behind the observed hippocampal-neocortical differences.

***SST-IN mediated inhibition and δOR activation exhibit similar hippocampal-neocortical divergence.***

A potential explanation for the absence of opioid modulation of neocortical PV-INs is that another neocortical interneuron subpopulation subserves this role. Somatostatin interneurons (SST-INs) comprise a substantial portion of MGE-derived interneurons[47], and within the HPC also express μORs and δORs, though with lower probability relative to PV-INs[29]. To explore the possibility that neocortical SST-INs are suppressed by opioids, we undertook similar optogenetic experiments in $SST^{Cre/+}$:$ChR2^{fl/+}$ mice (Fig. 3A-B). We observed that as with PV-INs, IeIPSCs from SST-INs within HPC were reversibly suppressed by DAMGO (Fig. 3C), whereas within S1 cortex, no such significant suppression was observed (Fig. 3D). Thus, SST-INs appear to exhibit a similar hippocampal specialization as PV-INs.

Also of interest is the role of δORs, as these are co-expressed in hippocampal PV-INs and SST-INs, and function through partially occlusive downstream pathways to hyperpolarize interneurons[27]. To assess whether δORs exhibit different regional functions from μORs, we performed similar optogenetic experiments in $PV^{Cre/+}$:$ChR2^{fl/+}$ mice, applying the δOR selective agonist DPDPE (500 nM) and antagonist naltrindole (100 nM) (Fig. 3E). As with μOR modulation, δOR modulation of PV-INs exhibited a similar regional divergence, with CA1 PV-INs suppressed by DPDPE (Fig. 3F), but no significant effect in V1 (Fig. 3G). Thus, the hippocampal-neocortical divergence in opioid suppression of inhibition appears to include μOR and δOR receptors, as well as other MGE-INs.

***Opioids selectively suppress hippocampal synaptic inhibition in nonhuman primates and resected human tissue.***

An ever-increasing number of transcriptional profiling studies highlight species divergence in neuronal genetic programs that may promote evolutionary innovations in neuronal/circuit properties[42,57,58]. To determine if opioid-mediated disinhibitory motifs are relevant in primate species, we turned to the study of rhesus macaques and resected human tissue. ISH RNAscope analysis of adult macaque tissue revealed that, consistent with rodents, the percentage of *Pvalb*+ cells co-expressing *Oprm1* was strongly enriched in CA1 (85.4 ± 4.7%), in contrast to neighboring temporal cortex (16.0 ± 5.3%, Fig. 4A-B). To functionally target PV-INs in macaques, we adopted a viral enhancer strategy. Adult macaques were

injected with AAV.PhP.Eb-S5E2-ChR2-mCherry in HPC or M1, acute slices prepared, and optogenetic experiments performed to record the effect of μOR drugs on IeIPSCs (Fig. 4C-D). As observed in mice, CA1 IeIPSCs were reversibly suppressed by DAMGO (Fig. 4E). CA3 IeIPSCs exhibited a long-lasting though non-significant DAMGO suppression, which was not easily reversed with CTAP or wash (Fig. 4F). In DG (Fig. 4G) and M1 (Fig. 4H), DAMGO elicited a highly variable response with no significant suppression. While this viral tool has been validated and shown to be specific to PV-INs in NHPs[44], we next confirmed that S5E2 cell inhibition functioned as expected from the mouse literature. We confirmed that S5E2 IeIPSCs were insensitive to 500 nM of the N-type $Ca^{2+}$ channel blocker ω-conotoxin (95.2 ± 6.7% of baseline, Fig. S4A), as expected from the mouse literature, as these presynaptic channels are primarily used by CCK-INs for neurotransmitter release[59,60]. In contrast, IeIPSCs from S5E2 cells were robustly suppressed by 250 nM of the P/Q-type $Ca^{2+}$ channel blocker ω-agatoxin (10.2 ± 4.3% of baseline, Fig. S4B), also expected from the mouse literature as murine PV-INs employ P/Q-type $Ca^{2+}$ channels for neurotransmitter release[60]. Moreover, S5E2 IeIPSCs were unaffected by 5 μM of the synthetic cannabinoid agonist WIN 55212-2 (97.2 ± 4.5% of baseline, Fig. S4C), which suppresses CCK-IN synaptic release through depolarization-induced suppression of inhibition (DSI)[61], in contrast to the observed effect of DAMGO (74.4 ± 2.8% of baseline, Fig. 4E). Thus, primate PV-INs appear to utilize similar synaptic mechanisms as in mice.

We next assessed the effect of DAMGO/CTAP on resected human tissue from patients with drug-resistant epilepsy (Fig. 4I). We recorded spontaneous IPSCs (sIPSCs) in CA-PCs (CA1 & CA3) and temporal cortex PCs (Fig. 4J). Although sIPSCs include GABAergic currents from all inhibitory interneurons, perisomatic-targeting fast-spiking PV-INs would be expected to be overly represented in this measure. Of note, several resections exhibited hippocampal sclerosis within CA1, observable as a marked reduction in the width of *str. pyr.* with few PCs available for patch clamp electrophysiology. Such sclerosis was likely related to the site of epileptogenesis, and sclerotic resections were not included for this study. Neighboring temporal cortical tissue was surgically removed to reach hippocampal structures and was not pathological. Notwithstanding these limitations, human sIPSCs exhibited a markedly similar regional divergence in DAMGO-mediated suppression, with a significant suppression in CA-PCs (Fig. 4K) and no suppression of CTX-PCs (Fig. 4L). Comparing across species, this hippocampal-neocortical divergence was remarkably well-conserved across mice (Fig. 4M), macaques (Fig. 4N), and humans (Fig. 4O). An emerging model for this observed difference is that hippocampal PV-INs are enriched in opioid receptors relative to neocortex, resulting in opioid-mediated hyperpolarization and presynaptic suppression of neurotransmission (Fig. 4P).

***Tac1 cells co-express PV and are suppressed by μOR agonists.***

We next explored whether PV-INs exhibit regional opioid divergence in early development. PV-IN function has traditionally been difficult to study in early development as PV itself is not well-expressed

until post-natal day (P)10 in mice[62]. We undertook an alternate approach from PV$^{Cre}$ mice, with the observation that tachykinin precursor 1 (Tac1, which with post-translational modification produces substance P and neurokinin A), is co-expressed in PV-INs[63,64]. To assess the utility of Tac1 as an interneuronal marker, we probed Tac1 in our Nkx2.1$^{Cre/+}$:Rpl22(RiboTag)$^{HA/HA}$ mice, observing that MGE-derived interneurons of both the hippocampus and neocortex are enriched in Tac1 compared to all neurons (Fig. 5A). To assess which MGE-IN subpopulation co-expresses Tac1, we immunohistochemically stained for PV in P5, P8, P12, and P45 Tac1$^{Cre/+}$:tdTomato$^{fl/+}$ mice (Fig. 5B-C). As previously reported, PV was minimally expressed in P5 and P8 mice, but was detectable within CA1 *str. pyr.* somata and perisomatic axonal terminals by P12. In contrast, Tac1 somata were readily detectable at all ages, with perisomatic axonal terminals detectable and colocalized with PV by P12. We quantified somatic colocalization by manually counting PV+ and Tac1+ cells across hippocampal and neocortical (S1) layers, observing that throughout CA1 layers, the percentage of PV-INs co-expressing Tac1 rapidly increased to 85.6 ± 2.4% by P12 (Fig. 5E, left), coinciding with the emergence of labeled PV-INs (Fig. 5F, left). CA1 PV co-expression with Tac1 was maintained in adulthood at 81.1 ± 2.0% (Fig. 5E, left). In all CA1 layers, the majority of PV cells co-expressed Tac1 (Fig. 5E, middle), with most PV cells (66%) and Tac1 cells (61%) residing in CA1 *str. pyr.* (Fig. 5F, middle). Likewise, the majority of PV cells co-expressed Tac1 in neocortical layers 2/3 (69.1 ± 5.8%) and 5/6 (64.0 ± 3.8%) (Fig. 5E, middle).

The inverse measure, the percentage of Tac1 cells that co-expressed PV, was somewhat lower, rising to ~50% throughout HPC and CTX in adulthood. Thus, the vast majority of PV cells co-express Tac1, but there appears to be a population of non-PV-expressing Tac1 cells. Notably, putative Tac1+ PCs were observed and readily distinguished by morphology and bright fluorescent labeling of dendrites, perhaps representing a limitation of the Tac1$^{Cre}$ line as they appeared clustered in irregular patches in a minority of sections (20/49 across all ages). Putative Tac1$_{PCs}$ represented a minority fraction, appearing only in principal cell layers and comprising 15% (CA1 *str. pyr.*), 17% (CA2 *str. pyr.*), 11% (CA3 *str. pyr.*), 11% (DG *gr.*), 12% (S1 L2/3) 9% (S1 L4), and 7% (S1 L5/6) of all Tac1+ labeled cells. However, their presence warrants caution if employing Tac1$^{Cre}$ mice for functional studies of immature PV-INs without isolating GABAergic activity or adopting an intersectional approach employing an additional Flp-recombinase marker. Additionally, as there is a reported subpopulation of Tac1-expressing SST-INs[65], we also stained for SST in the same mice (Fig. 5D). We observed only a small minority of SST cells co-expressing Tac1 and Tac1 cells co-expressing SST (5-8%, Fig. 5E-F, right). Together these data suggest that Tac1$^{Cre}$ mice, with some caveats, are a useful tool to study immature PV-IN function before the age of P10, when PV$^{Cre}$ mice are unreliable.

Utilizing Tac1$^{Cre/+}$:ChR2$^{fl/+}$ mice (Fig. 5G-I), we next explored if immature PV-IN mediated inhibition is modulated by opioids in early development. In P5-7 mice we observed that as in adults, GABAergic-isolated IeIPSCs within CA1 were reversibly suppressed by DAMGO (Fig. 5I). Within neocortex, we

observed that functional Tac1→PC light-evoked synaptic responses were often small and unreliable before the age of ~P8, thus we included in our study slightly older mice with a full age range from P6-13. Again, as in adults, we did not observe a significant suppression of immature PV-IN mediated inhibition in cortex. Thus, at the earliest timepoints just as PV-IN→PC synaptic connections are being formed, there is opioid receptor dependent modulation within the hippocampus not found in neocortex.

***Opioids and Tac1 cells regulate giant depolarizing potentials.***

During this critical period of the developing hippocampus, the principal network signature are giant depolarizing potentials (GDPs). These spontaneous synchronous events occur during a brief developmental window (P5-10) while GABA is depolarizing[66] and are believed to play an important role in hippocampal synaptogenesis[67]. To test the importance of opioids in regulating these events, we recorded spontaneous GDP associated currents (GDP-Is) intracellularly from CA3-PCs voltage-clamped to 0 mV to isolate GABAergic contributions, in which GDP-Is are readily detectable as conspicuously large outward events due to a barrage of $GABA_A$ currents (Fig. 5J). GDP-I rate was highly variable across brain slices, so to ensure a sufficient number of events for averaging we only considered slices with a GDP-I rate ≥ 2 events/min (30/52 slices). We next applied 100 nM DAMGO and observed a robust and reversible decrease in GDP-I event frequency (36 ± 8% of baseline, Fig. 5K). Thus, opioids have a previously unappreciated potent ability to suppress spontaneous network activity of the developing hippocampus, analogous to the effect of DAMGO on spontaneous sharp wave ripples (SWRs) in adulthood[45]. To determine if Tac1 cells could subserve this suppressing role, we optogenetically silenced Tac1 cells with $Tac1^{Cre/+}$:$ArchT^{fl/+}$ mice (Fig. 5L-M), observing that GDP-Is were significantly suppressed (66 ± 11% of baseline, Fig. 5N). Prior work from our lab identified MGE-INs as key regulators of GDP activity; optogenetically silencing MGE-INs reduces GDP-I frequency to 34 ± 6% of baseline[68]. Several studies have attributed GDP regulation and generation to dendritic-targeting SST-INs[69,70]. However, optogenetically silencing SST-INs results in only modest reductions of GDP-I frequency (71-80% of baseline)[71]. Thus, to account for the entire effects of DAMGO-mediated suppression and optogenetic MGE-IN silencing, other IN subpopulations likely contribute. This study presents for the first-time evidence that immature PV-INs play a key role in primordial hippocampal rhythmogenesis, an unsurprising result considering the essential role PV-INs play in adult hippocampal rhythmogenesis, and likely not previously reported due to the lack of a viable animal model to target these cells. The suppression of immature PV-INs by opioids at these early developmental time-points also has severe implications for the harmful aspects of opioid use on synaptogenesis and circuit development in the developing brain.

***Morphine pre-treatment occludes acute DAMGO suppression.***

μORs and δORs can become constitutively active, in which they activate G proteins even in the absence of agonist[72,73]. Believed to contribute to tolerance and dependence, exposure to exogenous

opioids results in a shift in μOR and δOR function to become more constitutively active in chronic[74] and withdrawal conditions[75,76]. Drug-induced alterations to the endogenous opioid system have not been well-studied in the hippocampus, though one early study found chronic morphine treatment results in altered RNA levels of *Penk* and *Gnas* (encoding the $G_{\alpha s}$ subunit of GPCRs)[77], although it is unclear if these changes are specific to distinct neuronal populations. Therefore, to determine if the opioid-mediated suppression of PV-INs is altered after morphine exposure, we injected morphine or saline in $PV^{Cre/+}$:$ChR2^{fl/+}$ mice prior to acute slice preparation and whole cell patch clamp recordings of IeIPSCs. We used three treatment regimens (Fig. 6A), each with an independent saline control group, including a bolus injection (15 mg/kg), a chronic treatment with increasing doses over 6 days (15, 20, 25, 30, 40, 50 mg/kg), and a withdrawal group receiving the chronic treatment but with acute slice preparation 72 hours instead of 1 hour after the final injection as with other groups. Optogenetic IeIPSC recordings were performed in CA1-PCs as previously described. As with un-injected mice (Fig. 2D-E), saline controls all exhibited significant DAMGO-mediated suppression of IeIPSCs (Fig. 6B). In morphine-injected mice, the acute DAMGO-mediated suppression was partially occluded, particularly in the withdrawal group for which DAMGO no longer significantly deviated from baseline (Fig. 6C). Comparing the normalized DAMGO response across all groups (Fig. 6D), the bolus and withdrawal groups exhibited a significant deviation from their saline control, which was somewhat moderated in the chronic group, potentially through long-term adaptations distinct from the withdrawal conditions where constitutive receptor activity has been described[75,76]. Although the physiological role of the opioid-mediated suppression of hippocampal PV-INs is not yet fully understood, these data indicate that this disinhibitory motif becomes dysregulated after morphine use. Exogenous opioids, in addition to well-described roles in analgesic and stress response, can therefore interfere with neuromodulation of hippocampal PV-INs, leading to disruption of rhythmic activity such as GDPs (Fig. 5), SWRs[45], and gamma oscillations[46], activities essential for learning and memory in the developing and adult brain.

## DISCUSSION

PV-INs are essential gatekeepers of cortical activity, supporting excitatory:inhibitory (E:I) balance, feedforward inhibition, gamma oscillations, SWRs, and as observed in this study, GDPs. The ability of opioids to suppress PV-IN activity has critical implications for their ability to perform these functions. This study demonstrates via electrophysiology, immunohistochemistry, and transcriptomics that outside of the hippocampus where the opioid-mediated suppression of PV-INs is well-documented, neocortical PV-INs largely do not express μOR receptors and are unaffected by μOR agonists. Consistent with these findings, early micro-iontophoresis studies observed that administration of the endogenous opioid enkephalin throughout CTX causes a net suppression of spiking activity, in contrast to the HPC where enkephalin promotes spiking activity via disinhibition[18,22]. IHC studies show that μOR-expressing neocortical cells are overwhelmingly GABAergic (97%), but primarily vasoactive intestinal peptide-expressing interneurons (VIP-INs, 92%) rather than PV-INs (8%)[78]. Intriguingly, neocortical μOR-expressing cells largely co-express Penk (preproenkephalin) the precursor to enkephalin, suggesting an auto-suppressing role of these cells. Within the hippocampus, VIP-INs are also the primary source of enkephalin[79], the release of which has been shown to support plasticity and social memory[80]. Thus, it appears that VIP-INs are the local source of endogenous opioids in both HPC and CTX, but the downstream receptor-expressing cells have diverged from PV/SST-INs in HPC to VIP-INs in CTX.

Contrasting with this dichotomy, some studies have found evidence for opioid-mediated suppression of PV-INs in select regions of neocortex. In the medial entorhinal cortex, inhibitory synaptic input from fast-spiking PV-INs can be suppressed by opioids, with a consequent increase in gamma oscillations [81]. In orbitofrontal cortex (OFC), electrical- and light-evoked PV-IN GABA release onto PCs display sensitivity to DAMGO in medial but not lateral OFC[82]. Within neighboring prelimbic cortex (PrL), morphine suppresses optogenetically-evoked PV-IN responses via μORs[83]. One possible explanation to reconcile these results with our own is that medial OFC is a phylogenetically older cortical region than lateral PFC[84], as are prelimbic cortex, entorhinal cortex, and allocortical HPC relative to other regions of neocortex. Potentially, these evolutionarily older structures exhibit region-specific transcriptomic, translational, or post-translational programs permitting the expression of functional μORs within PV-INs.

The developmental period of neurogenesis might contribute to this regional specificity, with earlier developing PV-INs exposed to unique factors enabling functional μOR expression. MGE-derived PV-INs are born during a protracted period of neurogenesis ranging from embryonic day (E)9.5-13.5[85]. However, MGE-derived hippocampal interneurons are born earlier, around E11.5[47], relative to the peak of neocortical PV-IN neurogenesis around E13.5[85,86]. In our own Tac1 experiments we observed that functional neocortical Tac1→PC synaptic connections were delayed relative to HPC, becoming prominent around P8, while within HPC they were robustly observed at the earliest ages studied (P5). Within the hippocampus, early-born E11.5 PV-INs are reported to express a higher level of PV, receive

a higher E:I synaptic ratio, and preferentially innervate dPCs over sPCs in contrast to late-born E13.5 PV-INs[87]. Within the SST-IN population, a subpopulation of early-born hub cells critically regulate GDPs[69,70]. Thus, the birth date of interneurons strongly determines circuit connectivity and function and, as has been suggested[88], may establish an additional criterion to classify neuronal populations. It remains to be demonstrated if the neurogenesis window of PV-INs contributes to the regional specificity of opioid modulation.

The energy demands of maintaining functional opioid receptors in hippocampal PV-INs suggests they support important physiological roles, and several have been suggested. Both the administration of exogenous opioids and endogenous opioid release promotes long-term potentiation (LTP) within the lateral perforant path to DG[89,90]. Within CA1, LTP is altered in rats chronically treated with morphine[91,92]. The specific PC sub-compartments innervated by opioid-sensitive inputs could also have profound effects on dendritic integration. Although we observed dendritic-targeting CA1 SST-INs to also be suppressed by opioids (Fig. 3A-C), as well as prior work demonstrating NPY-INs are suppressed by opioids[31], perisomatic-targeting PV-INs may be the greatest contributors to opioid-mediated disinhibition of PCs. In addition to expressing the highest levels of μORs[28,29], perisomatic inhibition targeting *str. rad*., *pyr*. and *or*. is more susceptible to opioid suppression relative to distal *str. l.m.*[93], suggesting that opioid-mediated disinhibition may bias a PC to preferentially integrate more proximal Schaffer collaterals relative to distal *str. l.m.* inputs. Opioids may also play a key role in place field formation, as during theta oscillations, a transient reduction in inhibition is critical for place field formation[94]. Future studies are needed to explore how learning, place field formation, and memory consolidation are affected by selective PV-IN modulation and opioid treatments in adult and developing animals.

The present study establishes that opioids are uniquely positioned to suppress hippocampal and not neocortical PV-INs. In contrast to reports of PV-IN evolutionary divergence[42,43], our data demonstrate this disinhibitory circuit motif is maintained across mice, macaques, and humans. This motif is established in early development, and both opioids and immature PV-INs critically regulate hippocampal rhythmogenesis, suggesting one potential mechanism for neurodevelopmental deficits due to chronic *in utero* opioid exposure[6]. These findings highlight that opioids acting through immature PV-INs have an underappreciated role in shaping hippocampal development.

## ACKNOWLEDGEMENTS

This work was supported by a NICHD Intramural Research Program (IRP) grant to CJM, NINDS IRP grant to KZ, NIMH IRP grant to BBA, and NIH Center on Compulsive Behaviors (CCB) fellowship to APC. This work was carried out in collaboration with the NIH Comparative Brain Physiology Consortium (CBPC) at the NIH IRP. RNA sequencing and analysis support was provided by the Molecular Genomics Core, Bioinformatics and Scientific Programming Core, NICHD. Imaging support was provided by Vincent

Schram at the NICHD Microscopy and Imaging Core. Support for mouse breeding and colony maintenance was provided by Daniel Abebe at NICHD.

## AUTHOR CONTRIBUTIONS

APC was responsible for project conceptualization, experimental design, electrophysiology experiments, imaging, analysis, and principal writer of this manuscript. KAP and CJM conceptualized, designed, and supervised the project. JHK, GV, RC, and KAP contributed to electrophysiology experiments. SK, AV, XY, and SH conducted IHC, ISH, and morphological reconstructions. VM conducted RiboTag experiments and analysis. EL assisted with morphine injections. MAGE, ACC, BEH, AP, AM, and BBA conducted NHP handling, injections, and surgery. KZ conducted surgical procedures with human patients. GF and JD provided support and design of viral constructs. All authors participated in drafting the manuscript. MAGE, BBA, KZ, and CJM provided critical resources for the study.

## DECLARATION OF INTERESTS

The authors declare no competing interests.

## FIGURES

***Fig. 1: μORs are enriched in and selectively hyperpolarize hippocampal PV-INs.***

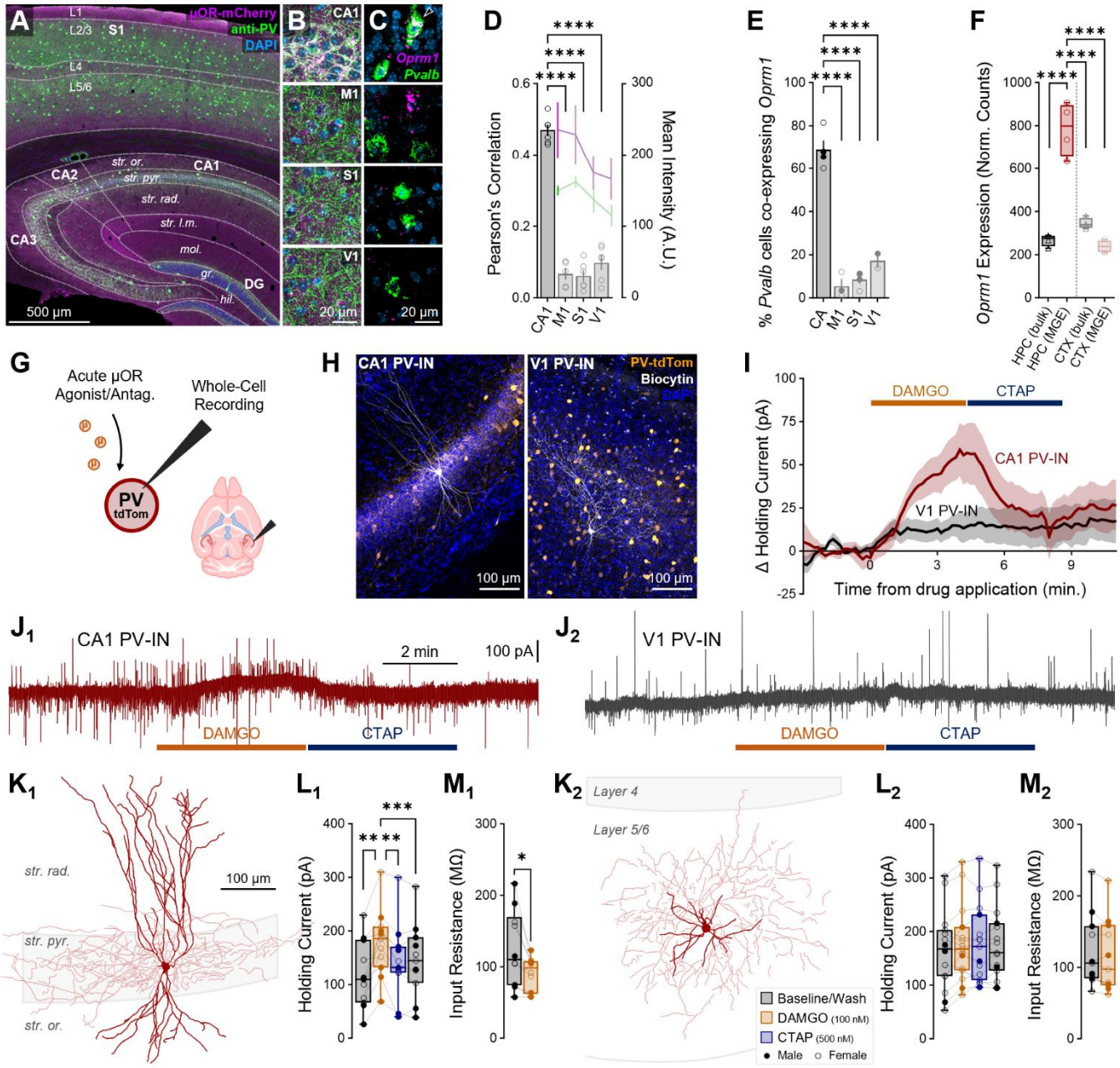


(**A**) Immunohistochemical (IHC) stain for PV in μOR-mCherry mice (boosted with anti-RFP) imaged with 20x confocal and (**B**) 63x Airyscan, labeling neocortical regions: S1, M1, and V1, and layers: L1, L2/3, L4, L5/6, hippocampal regions: CA1, CA2, CA3, and DG, CA layers: *stratum* (*str*.) *oriens* (*or*.), *pyramidale* (*pyr*.), *radiatum* (*rad*.), *lacunosum-moleculare* (*l.m.*), and DG layers: *molecular* (*mol*.), *granular* (*gr*.), *hilus* (*hil*.). (**C**) *In situ* hybridization (ISH) RNAscope for *Oprm1* and *Pvalb* in wild-type mice, same regions and scale as (*B*). Arrow indicates colocalized cell. (**D**) Quantification of IHC in (*B*) for $n_{section}$ = 6 from $n_{mice}$ = 2F, age = P70, P360 (P215 ± 145). Bars represent the average pixel-to-pixel Pearson's correlation

between the two channels. Asterisks represent Tukey's *post hoc* comparisons after a significant effect of region was observed via 1-way ANOVA, with the correlation in CA1 significantly higher than all cortical regions. Magenta/green lines represent the intensity of the *Oprm1*/*Pvalb* signals, with no differences observed between regions. (**E**) Quantification of percentage of *Pvalb*+ somata co-expressing *Oprm1* in ISH RNAscope in (*C*) for n = 4 (2F) wild-type mice, age = P62. Asterisks represent Tukey's *post hoc* comparisons after a significant effect of region was observed via 1-way ANOVA. (**F**) RiboTag-associated *Oprm1* expression in n = 4 (2F) Nkx2.1$^{Cre}$:Rpl22(RiboTag)$^{HA/HA}$ mice, age = P120, comparing bulk HPC/CTX tissue to MGE-INs. Asterisks represent Tukey's *post hoc* after significant effects of region and cell type were found via 2-way ANOVA. (**G**) Schematic of whole-cell recordings of PV-INs from PV-tdTom mice voltage-clamped to -50 mV to record the effect of μOR agonist/antagonist DAMGO/CTAP. (**H**) Representative *post hoc* staining of recorded PV-INs in CA1 and V1. (**I**) Average change in holding current elicited by DAMGO/CTAP normalized to baseline for $n_{cell}$ = 11 CA1 from $n_{mice}$ = 5 (3F), age = P37-70 (P57 ± 7) and $n_{cell}$ = 15 V1 from $n_{mice}$ = 4 (3F), age = P47-71 (P58 ± 6), with (**J**) example traces showing slow currents from drug administration and rapid sEPSCs/sIPSCs, (**K**) *post hoc* reconstructions, (**L**) holding current summary data, and (**M**) input resistance summary data in a subset of cells for CA1 PV-INs (**1***, left*) and V1 PV-INs (**2***, right*). Asterisks in (*L, M*) represent Tukey's *post hoc* comparisons after a significant effect of treatment was found via 1-way repeated measures ANOVA. Data are represented as mean ± SEM. In these and all subsequent plots, data from male subjects are indicated with a closed marker and data from females with an open marker. * $p < 0.05$, ** $p < 0.01$, *** $p < 0.001$, **** $p < 0.0001$. See Table S1 for statistical details.

***Fig. 2: Opioids selectively suppress hippocampal but not neocortical PV-IN inhibition.***

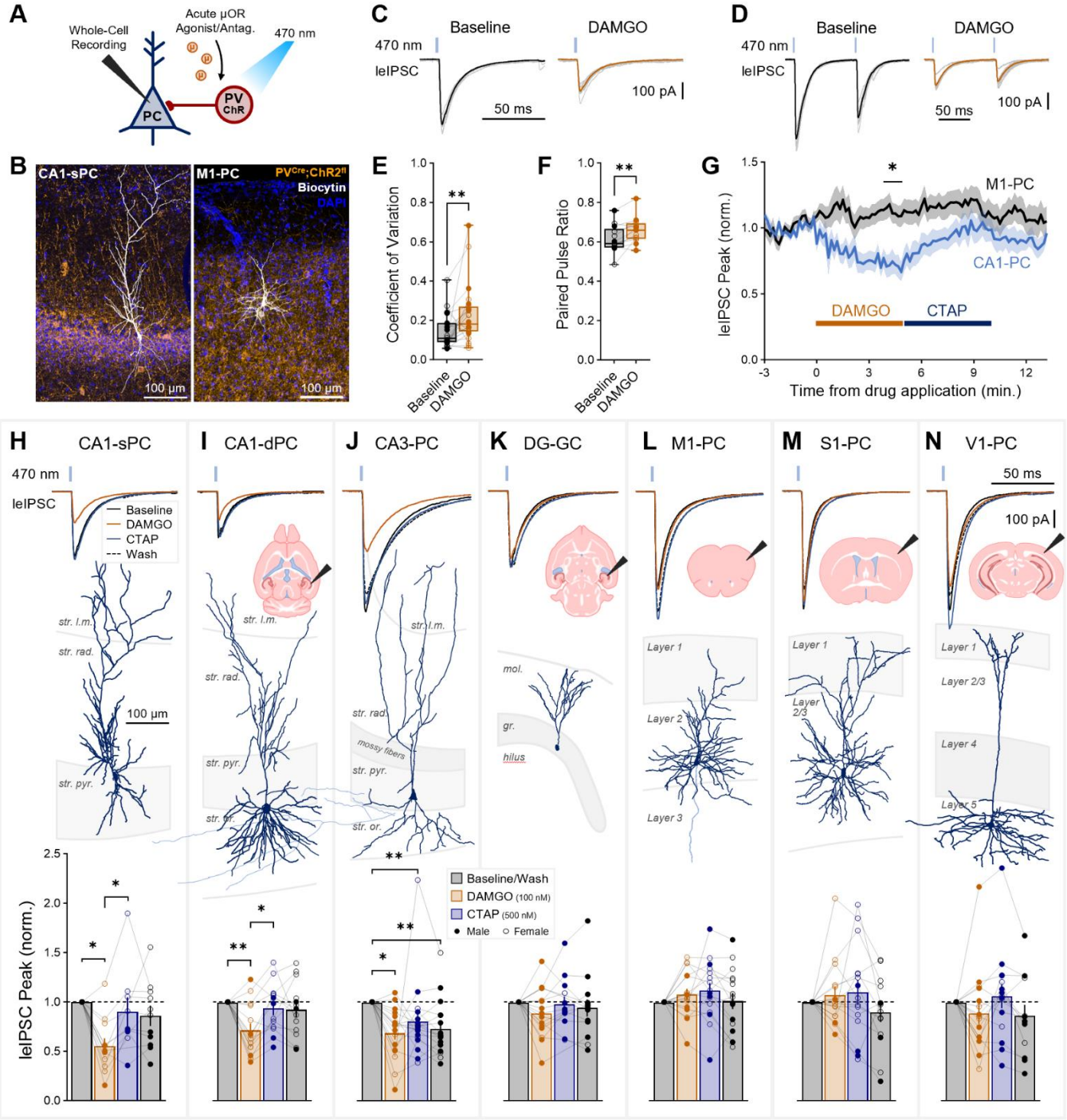


(**A**) Schematic of whole-cell recordings of PCs from $PV^{Cre/+}$:$ChR2^{fl/+}$ mice voltage-clamped at -70 mV (with high $Cl^-$ internal) to record the effect of DAMGO/CTAP on light-evoked IPSCs (IeIPSCs). (**B**) Representative *post hoc* staining of a recorded CA1 superficial PC (sPC) and M1 layer 2/3 PC. (**C**) Example CA1-PC IeIPSC traces, dark lines represent average of ten light grey traces, showing an increased coefficient of variation (CV = SD/mean). (**D**) Example paired pulse ratio (PPR = peak2/peak1) traces recorded in a subset of CA1-PCs. Summary data for (**E**) CV for $n_{cell}$ = 24 from $n_{mice}$ = 10 (5F), age

= P28-133 (P55 ± 9) and (**F**) PPR for $n_{cell}$ = 13 from $n_{mice}$ = 3 (2F), age = P78-83 (P80 ± 2). (**G**) Average IeIPSC peak amplitude in response to DAMGO/CTAP for $n_{cell}$ = 19 CA1-PCs from $n_{mice}$ = 7 (4F), age = P28-55 (P44 ± 3) and $n_{cell}$ = 16 M1-PCs from $n_{mice}$ = 6 (4F), age = P34-61 (P46 ± 5). Asterisk marks regions where data (10 s bins) survived multiple comparisons via 2-way ANOVA. (**H**-**N**) Mouse IeIPSC experiments with (*top*) averaged example traces, (*top inset*) example of brain slices, (*middle*) representative *post hoc* reconstructions, and (*bottom*) summary data in (**H**) $n_{cell}$ = 12 CA1-sPCs from $n_{mice}$ = 6 (3F), age = P28-133 (P62 ± 15), (**I**) $n_{cell}$ = 19 CA1 deep PCs (dPCs) from $n_{mice}$ = 9 (5F), age = P28-133 (P54 ± 10) (**J**) $n_{cell}$ = 17 CA3-PCs from $n_{mice}$ = 7 (2F), age = P41-80 (P65 ± 6) (**K**) $n_{cell}$ = 16 DG granule cells (GCs) from $n_{mice}$ = 9 (2F), age = P41-125 (P66 ± 10) (**L**) $n_{cell}$ = 16 M1-PCs from $n_{mice}$ = 6 (4F), age = P34-61 (P46 ± 5) (**M**) $n_{cell}$ = 15 S1-PCs from $n_{mice}$ = 4 (3F), age = P45-52 (P49 ± 2), and (**N**) $n_{cell}$ = 16 V1-PCs from $n_{mice}$ = 6 (2F), age = P27-133 (P73 ± 18). Data are represented as mean ± SEM. Asterisks in (*H-N*) summary plots represent *post hoc* comparisons (Tukey's/Dunn's) after a significant effect of treatment was found via 1-way repeated measure ANOVA/mixed model/Friedman's test. Data from male/female subjects are indicated with closed/open markers. * $p < 0.05$, ** $p < 0.01$. See Table S2 for statistical details.

***Fig. 3: SST inhibition and δOR activation exhibit similar hippocampal-neocortical divergence.***

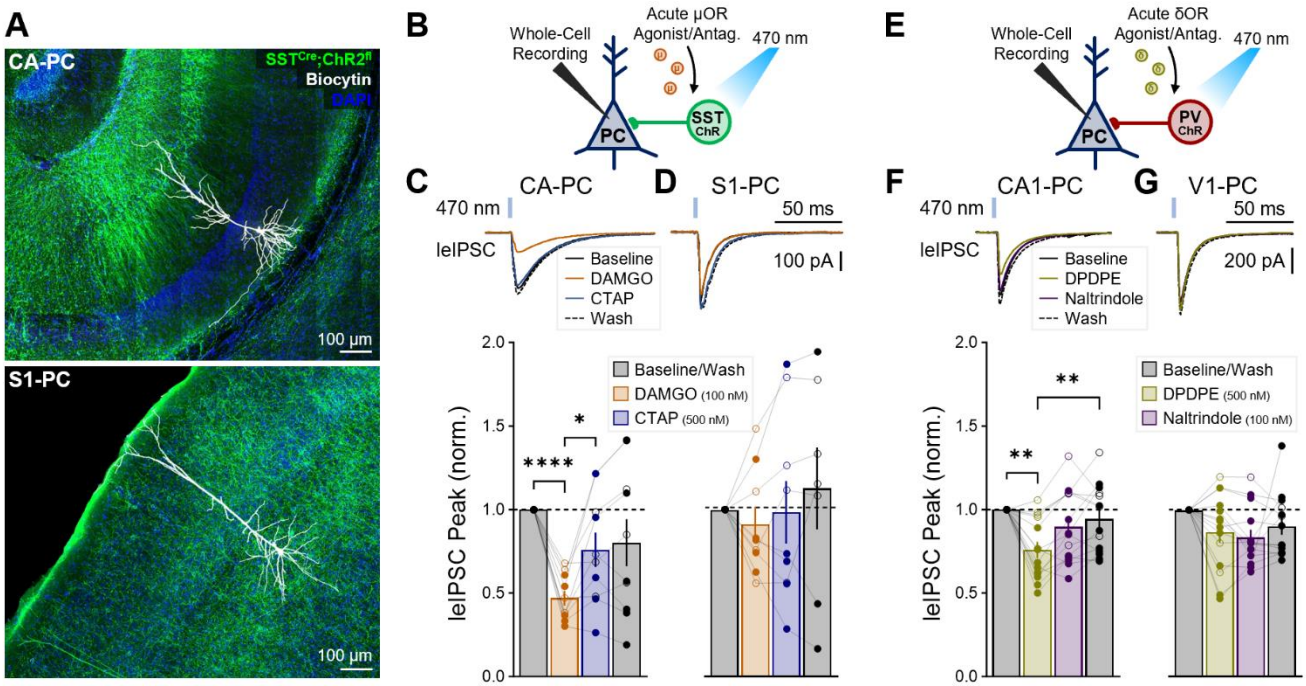


(**A**) Representative *post hoc* staining of recorded CA and S1 PCs in SST$^{Cre/+}$:ChR2$^{fl/+}$ mice. (**B**) Schematic of whole-cell recordings of PCs voltage-clamped at -70 mV (with high $Cl^-$ internal) to record the effect of DAMGO/CTAP on IeIPSCs. SST IeIPSC experiments were performed in (**C**) $n_{cell}$ = 10 CA-PCs from $n_{mice}$ = 3 (2F), age = P57-240 (P178 ± 61) and (**D**) $n_{cell}$ = 9 S1-PCs from $n_{mice}$ = 2 (1F), age = P240, P248 (P244 ± 4), with (*top*) averaged example traces and (*bottom*) summary data. (**E**) Schematic of whole-cell recordings of PCs recorded in PV$^{Cre/+}$:ChR2$^{fl/+}$ mice voltage-clamped at -70 mV (with high $Cl^-$ internal) to record the effect of δOR agonist/antagonist DPDPE/naltrindole on IeIPSCs. δOR IeIPSC experiments were performed in (**F**) $n_{cell}$ = 14 CA1-PCs from $n_{mice}$ = 5 (2F), age = P63-90 (P79 ± 4) and (**G**) $n_{cell}$ = 14 V1-PCs from $n_{mice}$ = 7 (2F), age = P57-90 (P73 ± 5), with (*top*) averaged example traces and (*bottom*) summary data. Data are represented as mean ± SEM. Asterisks represent Tukey's/Dunn's *post hoc* comparisons after a significant effect of treatment was found via 1-way repeated measure ANOVA/mixed model/Friedman's test. * $p < 0.05$, ** $p < 0.01$, **** $p < 0.0001$. Data from male/female subjects are indicated with closed/open markers. See Table S3 for statistical details.

***Fig. 4: Opioids selectively suppress hippocampal inhibition in nonhuman primates and resected human tissue.***

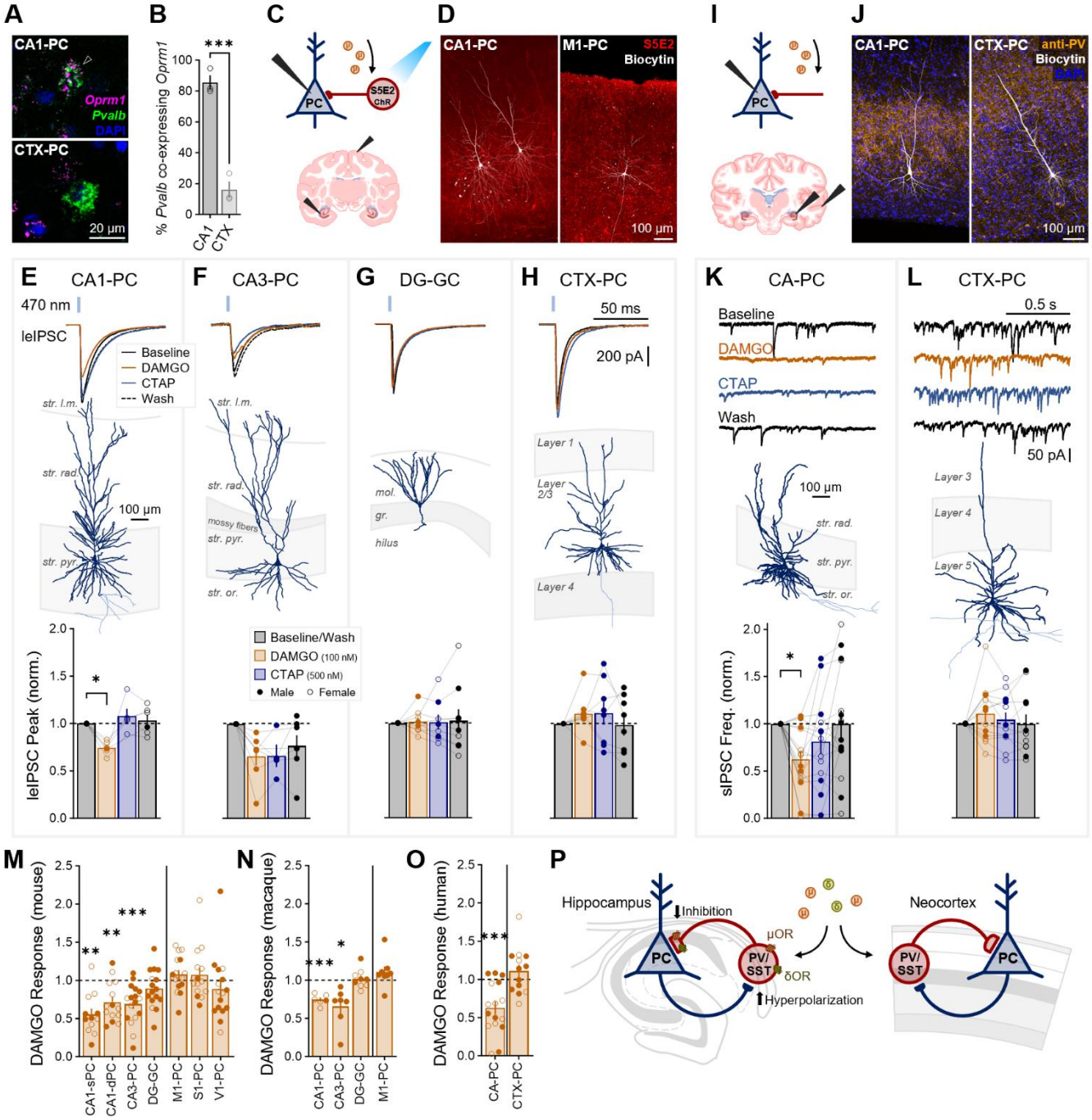


(**A**) RNAscope for *Oprm1* and *Pvalb* in adult rhesus macaque. Arrow indicates colocalized cell. (**B**) Quantification of the percentage of *Pvalb*+ somata co-expressing *Oprm1* for $n_{section}$ = 3 from 1F, age = 17.6 years. Asterisk represents unpaired t-test. (**C**) Schematic of whole-cell recordings of PCs from S5E2-ChR injected macaques voltage-clamped at -70 mV (with high $Cl^-$ internal) to record the effect of DAMGO/CTAP on IeIPSCs. (**D**) Representative *post hoc* staining of recorded CA1 and M1 PCs. (**E**-**H**) Macaque IeIPSC experiments with (*top*) averaged example traces, (*middle*) representative *post hoc*

reconstructions, and (*bottom*) summary data were performed in (**E**) $n_{cell}$ = 6 CA1-PCs from $n_{primate}$ = 1M, 1F, age = 15.9, 11.0 (13.5 ± 2.4) years, (**F**) $n_{cell}$ = 7 CA3-PCs from $n_{primate}$ = 1M, age = 15.9 years, (**G**) $n_{cell}$ = 9 DG-GCs from $n_{primate}$ = 1M, 1F, age = 15.9, 11.5 (13.7 ± 2.2) years, and (**H**) $n_{cell}$ = 8 M1-PCs from $n_{primate}$ = 2M, age = 7.4, 10.0 (8.7 ± 1.3) years. (**I**) Schematic of whole-cell recordings of PCs from resected human slices voltage-clamped at -70 mV (with high $Cl^-$ internal) to record the effect of DAMGO/CTAP on spontaneous IPSCs (sIPSCs). (**J**) Representative *post hoc* staining of a recorded CA1 and medial temporal cortex PC. (**K**-**L**) Human sIPSC experiments with (*top*) example traces, (*middle*) representative *post hoc* reconstructions, and (*bottom*) summary data were performed in (**K**) $n_{cell}$ = 16 CA-PCs (CA1 & CA3) from $n_{human}$ = 4 (2F), age = 42.7, 54.8, 37.3, 44.4 (44.8 ± 3.7) years and (**L**) $n_{cell}$ = 13 CTX-PCs from $n_{human}$ = 3 (2F), age = 54.8, 37.3, 44.4 (45.5 ± 5.1) years. Asterisks in (*E, K)* represent Tukey's *post hoc* comparisons after a significant effect of treatment was found via 1-way repeated measure ANOVA/mixed model. (**M**-**O**) Comparison of DAMGO responses across species revealed a similar hippocampal-neocortical divergence in the opioid-mediated suppression of inhibition across (**M**) mice (*data from Fig. 2H-N, bottom*), (**N**) macaques (*data from E-H, bottom*), and (**O**) humans (*data from K-M, bottom)*. (**P**) Proposed model: hippocampal PV-IN and SST-INs are selectively enriched in opioid receptors, leading to hyperpolarization and suppressed synaptic release. Asterisks in (*M-O*) represent significant deviations from the normalized baseline via 1-sample t-test/Wilcoxon. Data are represented as mean ± SEM. Data from male/female subjects are indicated with closed/open markers. * $p < 0.05$, ** $p < 0.01$, *** $p < 0.001$. See Table S4 for statistical details.

***Fig. 5: Tac1 cells, as a proxy for PV-INs in early development, are suppressed by μOR agonists and regulate giant depolarizing potentials.***

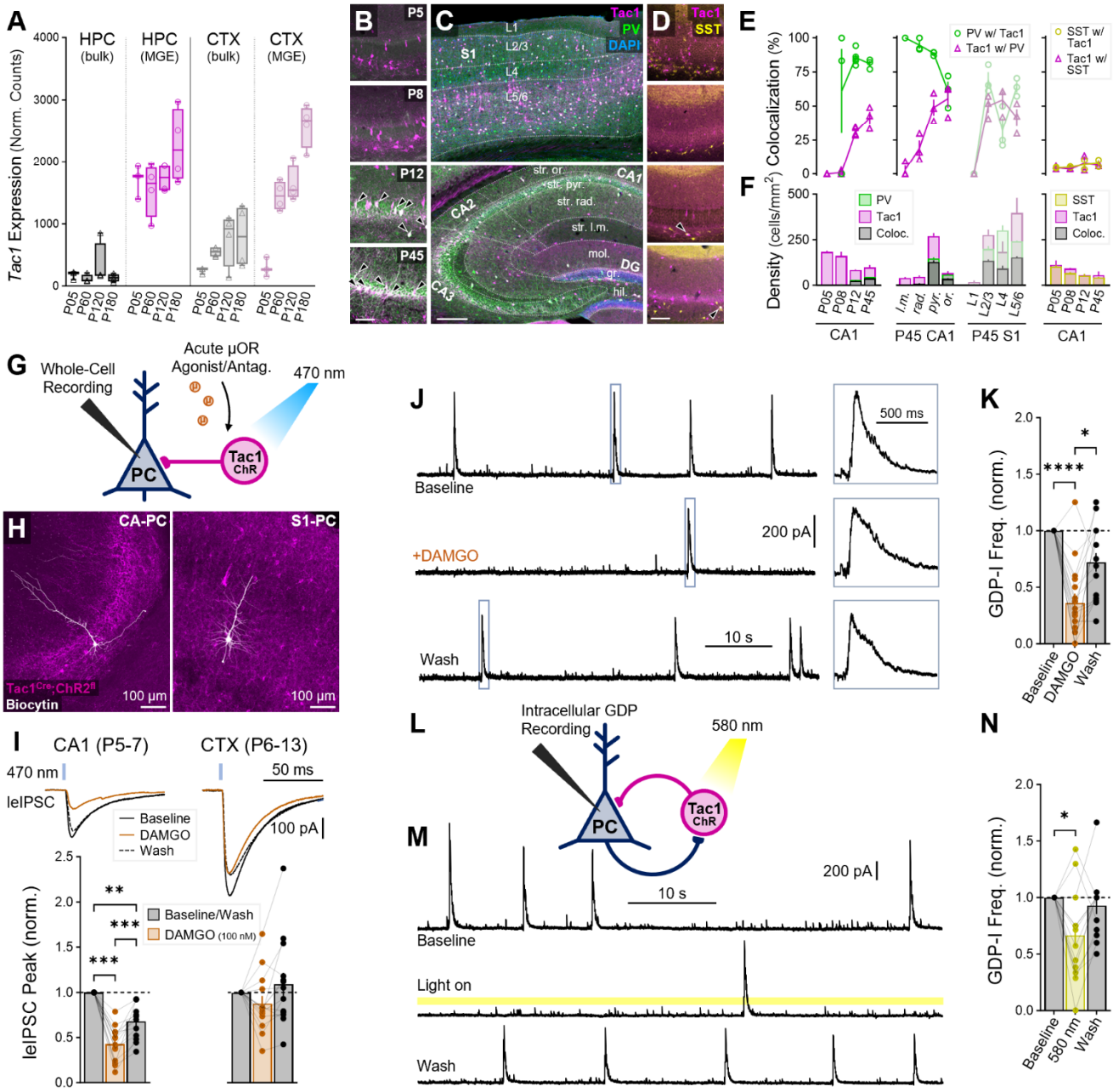


(**A**) RiboTag-associated *Tac1* expression in n = 4 (2F) P5, P60, P120, and P180 Nkx2.1$^{Cre}$: Rpl22(RiboTag)$^{HA/HA}$ mice, comparing bulk HPC/CTX tissue to MGE-INs. (**B-C**) IHC stain for PV in Tac1$^{Cre/+}$:tdTom$^{fl/+}$ mice, ranging from ages (**B**, *top to bottom*) P5, P8, P12, P45 in CA1, showing the developmental onset of PV expression and colocalization with Tac1, as well as (**C**) in P45 adults throughout S1 cortex (*top*) and HPC (*bottom*). (**D**) IHC stain for SST in Tac1$^{Cre/+}$:tdTom$^{fl/+}$ mice, same ages as *B*. Scale bars in *B*, *D* = 100 μm, *C* = 200 μm. Arrow indicate colocalized cells. Quantification of (**E**) percent colocalization and (**F**) cell density. *Left*: PV-Tac1 CA1 quantification, $n_{section}$ = 2-4 from $n_{mice}$ =

1 P5, 1 P8, 1 P12, and 3F P45. *Middle*: PV-Tac1 quantification for CA1 and S1 layers, $n_{mice}$ = 3F P45 (2-4 sections each). *Right*: SST-Tac1 CA1 quantification, $n_{section}$ = 2 from $n_{mice}$ = 1 P5, 1 P8, 1 P12, and 2F P45. (**G**) Schematic of whole-cell recordings of PCs recorded in Tac1$^{Cre/+}$:ChR2$^{fl/+}$ mice voltage-clamped at -70 mV (with high $Cl^-$ internal) to record the effect of DAMGO on IeIPSCs. (**H**) Representative *post hoc* staining of recorded PCs from CA and S1. (**I**) IeIPSC experiments were performed in $n_{cell}$ = 14 CA1-PCs from $n_{mice}$ = 3 (P5-7) and $n_{cell}$ = 14 CTX-PCs (from M1, S1, and V1) from $n_{mice}$ = 4 (P6-13), with (*top*) averaged example traces and (*bottom*) summary data. (**J**) Example traces of GDP associated currents (GDP-Is) recorded intracellularly in CA3-PCs voltage-clamped to 0 mV in WT mice, with 100 nM DAMGO applied for 5 minutes, with (*right inset*) example GDP-I events, and (**K**) summary data for $n_{cell}$ = 16 from $n_{mice}$ = 8 (P5-8). (**L**) Schematic of GDP-I recordings in Tac1$^{Cre/+}$:ArchT$^{fl/+}$ mice to silence Tac1 cells. (**M**) Example traces of GDP-Is recorded intracellularly in CA3-PCs. (**N**) Summary data for $n_{cell}$ = 14 from $n_{mice}$ = 7 (P5-8). Data are represented as mean ± SEM. Asterisks represent Tukey's/Dunn's *post hoc* comparisons after a significant effect of treatment was found via 1-way repeated measure ANOVA/Friedman's test. * $p < 0.05$, ** $p < 0.01$, *** $p < 0.001$, **** $p < 0.0001$. In adult subjects (≥ P45, *C-E*), data from male/female subjects are indicated with closed/open markers. Juveniles (P5-13) were not sexed. See Table S5 for statistical details.

***Fig. 6: Morphine pre-treatment occludes acute DAMGO suppression.***

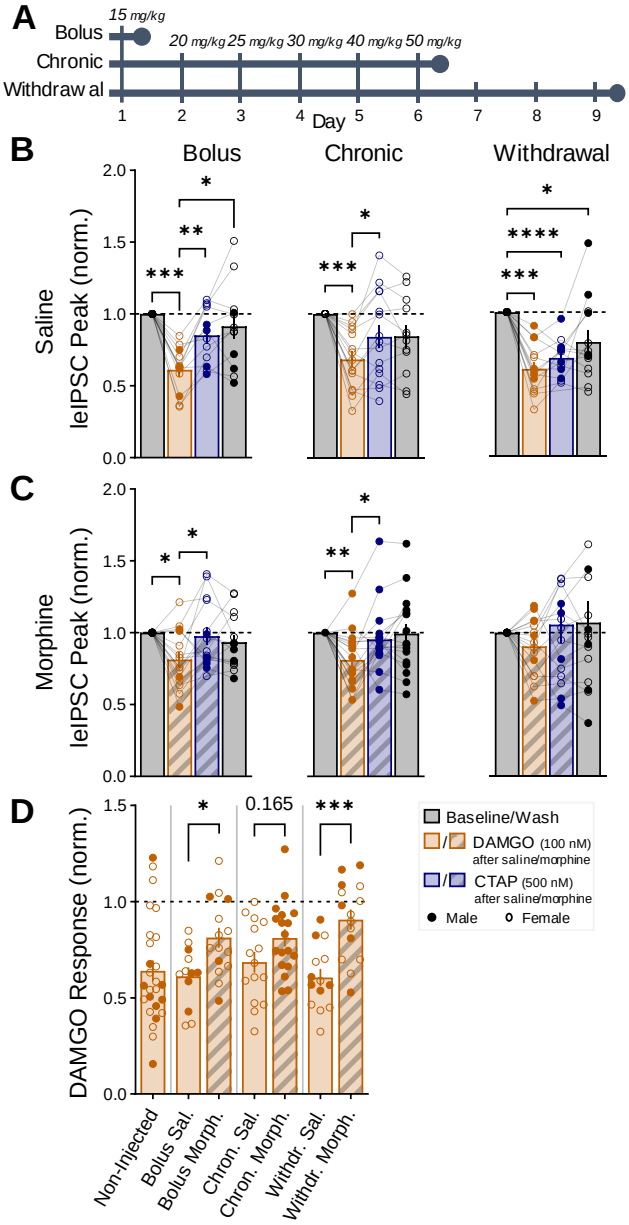


(**A**) Experimental design with 3 regimens: bolus (15 mg/kg), chronic (15, 20, 25, 30, 40, 50 mg/kg) and withdrawal (chronic regimen + 72 hours). All injections were performed in adult PV$^{Cre/+}$:ChR2$^{fl/+}$ mice with either daily morphine or saline injections, for a total of 6 groups. (**B**) Saline control groups all exhibited significant DAMGO suppression of IeIPSCs recorded in CA1-PCs (compare to *Fig. 2D-E*). *Bolus*: $n_{cell}$ = 12 from $n_{mice}$ = 3 (2F), age = P64-126 (P103 ± 20). *Chronic*: $n_{cell}$ = 15 from $n_{mice}$ = 3F, age = P67-76 (P73 ± 3). *Withdrawal*: $n_{cell}$ = 14 from $n_{mice}$ = 3 (2F), age = P78-83 (P80 ± 2). (**C**) Morphine injected groups exhibited partial occlusion of acute DAMGO-mediated suppression of IeIPSCs, particularly in the withdrawal group. Asterisks in (*B-C*) represent Tukey's *post hoc* comparisons after a significant effect of treatment was found via 1-way repeated measure ANOVA/mixed model. *Bolus*: $n_{cell}$ = 15 from $n_{mice}$ = 3 (2F), age = P65-127 (P104 ± 20). *Chronic*: $n_{cell}$ = 18 from $n_{mice}$ = 3M, age = P68-76 (P72 ± 2). *Withdrawal*: $n_{cell}$ = 15 from $n_{mice}$ = 3 (2F), age = P77-81 (P79 ± 1) (**D**) Combined DAMGO responses (non-injected data from *Fig. 2D-E* for comparison). Data are represented as mean ± SEM. Asterisks represent Šídák's *post hoc* comparisons after a significant effect of treatment was found via 2-way ANOVA, with comparisons restricted to those of *a priori* interest (morphine vs. saline for each regimen). * $p < 0.05$, ** $p < 0.01$, *** $p < 0.001$, **** $p < 0.0001$. See Table S6 for statistical details.

# METHODS

## *KEY RESOURCES TABLE*

| REAGENT or RESOURCE | SOURCE | IDENTIFIER |
|---|---|---|
| **Antibodies** | | |
| Rabbit anti-Parvalbumin | Abcam | Cat# ab11427, RRID:AB_298032 |
| Rabbit anti-Somatostatin 28 | Abcam | Cat# ab111912, RRID:AB_10903864 |
| Guinea Pig anti-RFP | Synaptic Systems | Cat# 390005, RRID:AB_2737051 |
| Rabbit anti-GFP | Abcam | Cat# ab290, RRID:AB_303395 |
| Rabbit anti-RFP | Antibodies-Online | Cat# ABIN129578, RRID:AB_10781500 |
| AF488 Goat anti-Rabbit IgG (H+L) | Thermo Fisher Scientific | Cat# A-11008, RRID:AB_143165 |
| AF555 Goat anti-Guinea Pig IgG (H+L) | Thermo Fisher Scientific | Cat# A-21435, RRID:AB_2535856 |
| AF488 Goat anti-Rabbit IgG (H+L) | Thermo Fisher Scientific | Cat# A-11034, RRID:AB_2576217 |
| AF555 Goat anti-Rabbit IgG (H+L) | Thermo Fisher Scientific | Cat# A-21429, RRID:AB_2535850 |
| **Bacterial and virus strains** | | |
| pAAV-PHP.eB-S5E2-ChR2-mCherry | Addgene[44] | RRID:Addgene_135634-PHPeB |
| **Chemicals, peptides, and recombinant proteins** | | |
| DAMGO | Tocris | Cat# 1171 |
| CTAP | Tocris | Cat# 1560 |
| DPDPE | Tocris | Cat# 1431 |
| Naltrindole hydrochloride | Millipore Sigma | Cat# N115 |
| DNQX disodium salt | Tocris | Cat# 2312 |
| DL-APV | Tocris | Cat# 0105 |
| CGP 55845 hydrochloride | Tocris | Cat# 1248 |
| ω-Agatoxin IVA | Tocris | Cat# 2799 |
| ω-Conotoxin GVIA | Tocris | Cat# 1085 |
| WIN 55212-2 mesylate | Tocris | Cat# 1038 |
| Biocytin | Millipore Sigma | Cat# B4261 |
| AF488 streptavidin | Thermo Fisher Scientific | Cat# S11223 |
| AF555 streptavidin | Thermo Fisher Scientific | Cat# S21381 |
| DAPI | Millipore Sigma | Cat# D9542 |
| RNAscope mouse probe Mm-Pvalb | Advanced Cell Diagnostic | Cat# 421931 |
| RNAscope mouse probe Mm-Oprm1-C2 | Advanced Cell Diagnostic | Cat# 315841-C2 |
| RNAscope macaque probe Mmu-PVALB | Advanced Cell Diagnostic | Cat# 461691 |
| RNAscope macaque probe Mmu-OPRM1-C2 | Advanced Cell Diagnostic | Cat# 518941-C2 |
| Opal 520 | AKOVA | Cat# OP-001001 |
| Opal 570 | AKOVA | Cat# OP-001003 |
| ProLong Diamond Antifade Mountant with DAPI | Thermo Fisher Scientific | Cat# P36962 |
| ProLong Gold Antifade Mountant | Thermo Fisher Scientific | Cat# P10144 |
| Morphine Sulfate Injection, USP (4 mg/mL) | Hikma Pharmaceuticals | NDC:0641-6125 |
| **Critical commercial assays** | | |
| RNAscope Multiplex Fluorescent v2 Assay | Advanced Cell Diagnostic | Cat#: 323110 |
| RNeasy Plus Micro Kit | Qiagen | Cat# 74034 |
| RNA 6000 Pico kit | Agilent | Cat# 5067-1513 |
| SMARTer Stranded Total RNA-Seq. Kit v2 | Takara Bio | Cat# 634411 |
| **Experimental models: Organisms/strains** | | |

| | | |
|---|---|---|
| Mouse: PV$^{Cre/Cre}$ | Jax[95] | RRID:IMSR_JAX:017320 |
| Mouse: SST$^{Cre/Cre}$ | Jax[96] | RRID:IMSR_JAX:013044 |
| Mouse: Tac1$^{Cre/Cre}$ | Jax[97] | RRID:IMSR_JAX:021877 |
| Mouse: Nkx2.1$^{Cre/Cre}$ | Jax[98] | RRID:IMSR_JAX:008661 |
| Mouse: tdTomato(Ai9)$^{fl/fl}$ | Jax[99] | RRID:IMSR_JAX:007909 |
| Mouse: ChR2(Ai32)$^{fl/fl}$ | Jax[100] | RRID:IMSR_JAX:024109 |
| Mouse: ArchT(Ai40D)$^{fl/fl}$ | Jax[101] | RRID:IMSR_JAX:021188 |
| Mouse: Rpl22(RiboTag)$^{HA/HA}$ | Jax[48] | RRID:IMSR_JAX:011029 |
| Mouse: μOR-mCherry | Jax[35] | RRID:IMSR_JAX:029013 |
| Mouse: PV-tdTomato | Jax | RRID:IMSR_JAX:027395 |
| **Software and algorithms** | | |
| pClamp 10.7 | Molecular Devices | RRID:SCR_011323 |
| FIJI (ImageJ) | NIH | RRID:SCR_002285 |
| Excel | Microsoft | RRID:SCR_016137 |
| Prism | Graphpad | RRID:SCR_002798 |
| ZEN Microscopy Software | Zeiss | RRID:SCR_013672 |
| SPOT Basic 5.2 | SPOT Imaging | RRID:SCR_014313 |
| DESeq2 | Bioconductor[102] | RRID:SCR_015687 |
| FIJI Macro: colocIHC | this manuscript | https://doi.org/10.5281/zenodo.10063200 |

## *RESOURCE AVAILABILITY*

### *Lead Contact*

Further information and requests for resources and reagents should be directed to and will be fulfilled by the lead contact, Adam Caccavano (adam.caccavano@nih.gov).

### *Materials Availability*

This study did not generate novel, unique reagents.

### *Data and Code Availability*

Data generated during this study are available upon request. The custom ImageJ macro developed to automate IHC colocalization is open-source and available via public repositories: a current version subject to change (https://github.com/acaccavano/colocalizationIHC) and an archival copy used for this manuscript (https://doi.org/10.5281/zenodo.10063200).

## *EXPERIMENTAL MODEL AND STUDY PARTICIPANT DETAILS*

### *Mice*

Targeted fluorescent labeling of neuronal subpopulations was achieved through Cre-recombinase driven expression of floxed reporters, with experimental offspring maintained as heterozygous crosses of homozygous Cre-recombinase drivers PV$^{Cre/Cre}$ (RRID:IMSR_JAX:017320)[95], SST$^{Cre/Cre}$

(RRID:IMSR_JAX:013044)[96], Tac1$^{Cre/Cre}$ (RRID:IMSR_JAX:021877)[97], Nkx2.1$^{Cre/Cre}$ (RRID:IMSR_JAX:008661)[98] and homozygous floxed reporters tdTomato(Ai9)$^{fl/fl}$ (RRID:IMSR_JAX:007909)[99], ChR2(Ai32)$^{fl/fl}$ (RRID:IMSR_JAX:024109)[100], ArchT(Ai40D)$^{fl/fl}$ (RRID:IMSR_JAX:021188)[101], and Rpl22(RiboTag)$^{HA/HA}$ (RRID:IMSR_JAX:011029) [48]. Notably, Nkx2.1$^{Cre/+}$:Rpl22(RiboTag)$^{HA/+}$ offspring were cross-bred for several generations to obtain homozygosity in Rpl22$^{HA/HA}$, to account for the relatively low expression of the endogenous *Rpl22* gene[49,50]. To characterize μOR expression, we employed μOR-mCherry$^{+/-}$ transgenic mice (RRID:IMSR_JAX:029013)[35]. Direct recordings of PV-INs were performed in PV-tdTomato$^{+/-}$ mice (RRID:IMSR_JAX:027395). Male and female mice were used in approximately equal number. In this way, the total experimental mice used for this study were: 57 (26F) PV$^{Cre/+}$:ChR2$^{fl/+}$, 11 Nkx2.1$^{Cre/+}$:Rpl22(RiboTag)$^{HA/HA}$, 9 (6F) PV-tdTomato$^{+/-}$, 7 Tac1$^{Cre/+}$:ChR2$^{fl/+}$, 7 Tac1$^{Cre/+}$:ArchT$^{fl/+}$, 6 Tac1$^{Cre/+}$:tdTomato$^{fl/+}$, 4 (2F) SST$^{Cre/+}$:ChR2$^{fl/+}$, 2F μOR-mCherry$^{+/-}$, and 6 wild-type mice. Mice were housed and bred in a conventional vivarium with standard laboratory chow and water in standard animal cages under a 12 hr circadian cycle.

***Nonhuman Primates (NHPs)***

All experiments were performed in accordance with the ILAR Guide for the Care and Use of Laboratory Animals and were conducted under an Animal Study Protocol approved by the ACUC at the National Institute of Mental Health. All procedures adhered to the applicable Federal and local laws, regulations, and standards, including the Animal Welfare Act and Regulations and Public Health Service policy (PHS2002). Tissue was obtained from 6 adult rhesus macaques (3F), aged 7 – 18 (12.2 ± 1.5) years, that had reached the end of their paradigms for other experiments, as part of the NIH comparative brain physiology consortium (CBPC).

An AAV.PhP.Eb virus carrying a ChR2-mCherry fusion protein expressed under an S5E2 promoter (AAV.PhP.Eb-S5E2-ChR2-mCherry, ≥ $7\times10^{12}$ viral genomes/mL) was injected into the left HPC of 3 rhesus macaques. 20-25 μL of virus was injected at each of 2 locations spaced approximately 2 mm apart in the antero-posterior plane, caudal to the level of the uncus. Injections were targeted using stereotaxic coordinates derived from MRI and delivered using a needle guide for enhanced accuracy[103]. 30-40 μL of virus was injected into M1 of 2 rhesus macaques. 10 μL of virus was injected at each of 3-4 locations spaced approximately 2 mm apart, targeted via direct visualization. Surgeries were performed under aseptic conditions in a fully equipped operating suite.

For brain extraction, 6-8 weeks after virus injection, animals were sedated with ketamine/midazolam (ketamine 5-15 mg/kg, midazolam 0.05-0.3 mg/kg) and maintained on isoflurane. A deep level of anesthesia was verified by an absence of response to toe-pinch and absence of response to corneal reflex. Prior to brain removal and blocking the animals were transcardially perfused with ice-cold sucrose-substituted artificial cerebrospinal fluid (aCSF) containing in mM: 90 Sucrose, 80 NaCl, 3.5 KCl, 1.25

$NaH_2PO_4$, 24 $NaHCO_3$, 10 Glucose, 0.5 CaCl, 4.5 $MgCl_2$ saturated with carbogen (95% $O_2$, 5% $CO_2$), with osmolarity 310-320 Osm.

***Human Tissue***

Human tissue was obtained from surgical specimens collected from 5 (2F) anonymized/deidentified patients with pharmaco-resistant epilepsy, aged 37-54 (44.9 ± 2.8) years. The participants underwent an initial surgical procedure during which recording electrodes were implanted subdurally on the cortical surface and within the brain parenchyma to monitor epileptiform activity. The location of the intracranial electrodes was selected by the clinical team to localize the epileptogenic zone and recordings during a monitoring period were used to identify the specific hippocampal region exhibiting ictal or inter-ictal activity. During a second surgery the brain areas of seizure onset were surgically resected. The Institutional Review Board (IRB) at the National Institute of Neurological Disease and Stroke approved the research protocol and informed consent for the experimental use of surgically resected tissue was obtained from each participant and their guardian.

***METHOD DETAILS***

***Acute Slice Electrophysiology***

Mice were anesthetized with isoflurane and rapidly decapitated. Brains were dissected, blocked, and sectioned in iced sucrose-substituted aCSF. Horizontal or coronal slices (300 µm) were sectioned a VT-1200S vibratome (Leica Microsystems), then transferred to a submerged incubation chamber containing oxygenated warmed (32-34 °C) sucrose-substituted aCSF for 30 minutes then maintained at room temperature for the duration of the day. Slices were allowed to recovery post-sectioning for at least 1 hour before transfer to the recording chamber. NHP and human samples were sectioned identically but were maintained for up to 72 hours in room temperature oxygenated sucrose-substituted aCSF, with solution changes every 24 hours.

Slices were transferred to an upright microscope (Olympus BX51Wl) and perfused with oxygenated extracellular aCSF containing in mM: 130 NaCl, 3.5 KCl, 1.25 $NaH_2PO_4$, 24 $NaHCO_3$, 10 Glucose, 2.5 CaCl, 1.5 $MgCl_2$, with osmolarity 300-310 Osm, with a flow rate of 2-3 mL/min at a temperature of 30-33 °C. Individual cells were visualized with a 40x objective using fluorescence and IR-DIC microscopy. Electrodes were pulled from borosilicate glass (World Precision Instruments) to a resistance of 3-5 MΩ with a vertical pipette puller (Narishige PC-10). Whole-cell patch-clamp recordings were made with a Multiclamp 700B amplifier (Molecular Devices), with signals digitized at 20 kHz (Digidata 1440A, filtered at 3 kHz). Recordings were made using a Windows 10 computer with pClamp 10.7 (Molecular Devices). In voltage-clamp recordings, uncompensated access resistance ($R_A$) was monitored consistently with 5 mV voltage steps. Any recordings in which $R_A$ deviated by more than 20% were discarded.

Direct response to opioids were recorded in fluorescently-identified cells with a standard K-Gluconate internal containing in mM: 150 K Gluconate, 0.5 EGTA, 3 $MgCl_2$, 10 HEPES, 2 ATP•Mg, 0.3 GTP•$Na_2$, and 0.3% biocytin (pH corrected to 7.2 with KOH, 285-290 Osm). Cells were held in voltage-clamp at -50 mV, and 100 nM DAMGO (μOR agonist) and 500 nM CTAP (μOR antagonist) applied.

Recordings of inhibitory light-evoked and spontaneous inhibitory post-synaptic currents (leIPSCs and sIPSCs) were made in visually-identified PCs held in voltage-clamp at -70 mV, with a high $Cl^-$ K-Gluconate internal (calculated $Cl^-$ reversal = -24 mV), containing in mM: 100 K Gluconate, 50 KCl, 0.5 EGTA, 3 $MgCl_2$, 10 HEPES, 2 ATP•Mg, 0.3 GTP•$Na_2$, 4 QX314, and 0.3% biocytin (pH corrected to 7.2 with KOH, 285-290 Osm). A brief (0.5-2 ms) 470 nm light pulse was illuminated on a small patch surrounding the recorded cell every 10 s. The light intensity was kept consistent between cells as much as possible, but as every recording was internally normalized to baseline, greater importance was placed on ensuring the leIPSC amplitude was detectable above noise and non-saturating (100-1000 pA). $GABA_A$ currents were isolated by washing into the bath 10 μM DNQX, 50 μM DL-APV, and 1 μM CGP 55845, to eliminate the contributions of AMPA, NMDA, and $GABA_B$ receptors, respectively. After a stable baseline was reached (5 min), the opioid drugs of interest were applied in the following nM concentrations: 100 DAMGO, 500 CTAP, 500 DPDPE (δOR agonist), and 100 Naltrindole (δOR antagonist). Each drug was applied for at least 5 min. Opioid concentrations were selected from prior publications[25,53]. Detailed dose-response experiments were not conducted.

Giant depolarizing potential associated currents (GDP-Is) were recorded intracellularly, by recording visually-identified CA3-PCs voltage-clamped to 0 mV in K-Gluconate. Optogenetic inactivation of Tac1 cells was achieved by sustaining a light pulse for 2-3 min at 580 nm in ArchT-expressing mice.

All electrophysiology analysis was conducted in Clampfit 10.7 (Molecular Devices) and organized/averaged in Microsoft Excel. Current responses to drugs recorded in PV-INs were calculated as the final 2 min average for each drug condition. leIPSC amplitudes recorded in PCs were calculated as the final ten sweep average for each drug condition. sIPSCs were detected using a template search and averaged for the final 2 min of each drug condition. GDP-Is were detected using a threshold set above spontaneous sIPSCs and with a minimum event duration of 25 ms. GDP-Is were quantified for the final 2 min of each drug condition, and only recordings with a rate ≥ 2 events/min in the baseline period were included.

***Immunohistochemistry (IHC)***

For mice younger than P10, brain tissues were dissected and drop fixed in 4% paraformaldehyde (PFA) for 24 hours at 4 °C. Mice older than P10 were transcardially perfused using 4% PFA and dissected brain tissues were post-fixed in 4% PFA for 24 hours at 4 °C. Fixed brain tissues were thoroughly washed in 1x phosphate buffer (PB) followed by cryopreservation using 30% sucrose. 50 μm coronal sections

were made on a frozen microtome. Brain slices were washed with 1x PB at room temperature for 1 hour with 2-3 changes of 1x PB. To perform floating section IHC, brain slices were blocked and permeabilized in Blocking Solution (1x PB + 10% goat serum + 0.5% Triton X-100) at room temperature for at least 2 hours. Primary antibodies were diluted using Antibody Solution (1x PB + 1% goat serum + 0.1% Triton X-100). Blocked brain slices were incubated in primary antibodies at 4 °C for 48 hours. After wash with 1x PB at room temperature for 15 minutes with 3 repeats, brain slices were incubated in secondary antibodies diluted with Antibody Solution at room temperature for 1 hour. After washed with 1x PB at room temperature for 15 minutes with 3 repeats, brain slices were mounted on gelatin coated slides followed by air drying, cover-slipped with Prolong Diamond Antifade mountant with DAPI (ThermoFisher Scientific Cat# P36962), cured in darkness, and imaged.

Primary antibodies and working dilution: rabbit anti-parvalbumin (Abcam Cat# ab11427, RRID:AB_298032) 1:1000; rabbit anti-somatostatin 28 (Abcam Cat# ab111912, RRID:AB_10903864) 1:1000; guinea pig anti-RFP (Synaptic Systems Cat# 390005, RRID:AB_2737051) 1:1000. Secondary antibodies and working dilution: Alexa Fluor 488 conjugated goat anti-rabbit IgG (Thermo Fisher Scientific Cat# A-11008, RRID:AB_143165) 1:1000; Alexa Fluor 555 conjugated goat anti-guinea pig IgG (Thermo Fisher Scientific Cat# A-21435, RRID:AB_2535856) 1:1000.

***Morphological Reconstruction***

Slices containing biocytin filled cells were dropped fixed in 4% PFA overnight at 4 ºC. Fixed slices were then washed in PBS, permeabilized with 0.3% Triton X-100 and incubated with Alexa-488 or Alexa-555 conjugated streptavidin overnight (Thermo Fisher Scientific, Cat# S11223, S21381). When additional staining was desired, tissue was incubated in Blocking Solution (Carrier Buffer + 10% goat serum + 0.5% Triton X-100) at room temperature for at least 2 hours. Primary antibodies were diluted using Carrier Buffer (1% bovine serum albumin + 1% goat serum in PBS) containing 0.5% Triton X-100 for 3 hours at room temperature. After washing with 1x PBS at room temperature for 15 minutes with 3 repeats, tissue was incubated with secondary antibodies diluted with Carrier Buffer and Triton at room temperature for 2 hours. After incubation, slices were incubated in 1 µg/ml DAPI (Millipore Sigma, Cat# D9542), then underwent multiple washes, cryopreserving in 30% sucrose and were resectioned to 70 µm using a freezing microtome (Microm, Whaltham, MA). Slices were then mounted on glass slides (Fisher Scientific, Fisherbrand Superfrost Plus) using Mowiol as a mounting medium. Confocal images of labelled cells were attained on a Zeiss LSM 710 microscope using a 20x objective.

Primary antibodies and working dilutions: rabbit anti-parvalbumin (Abcam, Cat# ab11427) 1:1000; rabbit anti-GFP (Abcam, Cat# ab290) 1:1000; rabbit anti-RFP (Antibodies-online, Cat# ABIN129578) 1:1000. Secondary antibodies and working dilution: Alexa Fluor 488 conjugated goat anti-rabbit IgG

(Fisher Scientific, Cat# A-11034) 1:1000; Alexa Fluor 555 conjugated goat anti-rabbit IgG (Fisher Scientific, Cat# A-21429) 1:1000.

***In situ Hybridization (ISH) RNAscope***

To prepare snap frozen tissue for ISH, freshly dissected brains or brain blocks were submerged into 2-methylbutane that was pre-chilled on a dry ice/ethanol bath for 1 minute. Tissue was removed, wrapped in foil, and stored at -80 °C. 10 µm frozen sections were made using a Leica Cryostat, mounted on slides (ThermoFisher Scientific) and stored at -80 °C.

Target probes were designed and manufactured by Advanced Cell Diagnostic (ACD): Mm-Pvalb (Cat# 421931), Mm-Oprm1-C2 (Cat# 315841-C2), Mmu-PVALB (Cat# 461691), Mmu-OPRM1-C2(Cat# 518941-C2). ISH was performed following the RNAscope Multiplex Fluorescent v2 Assay instructions provided by ACD. Briefly, frozen thin sections were post-fixed in 4% PFA and dehydrated sequentially in 50%, 70% and 100% ethanol. After $H_2O_2$ and Protease IV treatment, sections were incubated with probes at 40 °C for 2 hours. Probed signals were detected using RNAscope Multiplex Detection v2 kit (ACD, Cat# 323110). Opal 520 (AKOVA, Cat# OP-001001) and Opal 570 (AKOVA, Cat# OP-001003) were used to detect C1 and C2 probes, respectively. After DAPI staining, sections were covered using ProLong Gold Antifade Mountant (ThermoFisher Scientific, Cat# P10144) and cured in darkness before imaging.

***IHC and ISH Image Acquisition and Analysis***

IHC Images were captured on a Zeiss LSM 900 (confocal 20x and Airyscan 63x) and an Olympus VS200 slide scanner. Quantified images were captured from 2-5 sections for each subject. Microscope settings were kept consistent for all sections from each subject. Lower resolution confocal (20x) images used a broad z-stack (5 slices every 1.1 µm) which were maximum projected before subsequent analysis. High resolution Airyscan (63x) images used a detailed z-stack (60-70 slices every 0.15 µm), with subsequent correlation analysis performed on each individual slice and then averaged. RNAscope images were first acquired on a SLIDEVIEW VS200 slide scanner (Olympus) mounted with an ORCA-Fusion Digital Camera (HAMAMATSU). Hippocampal and neocortical regions were scanned at 20x, guiding subsequent 63x confocal z-stack images at regions of interest (ROIs).

For each 20x image, polygonal ROIs were drawn to demarcate hippocampal/neocortical layers and subregions. Mean intensity and correlation for each ROI were then computed by a custom ImageJ (FIJI) macro (see Data and Code Availability). A rolling ball background subtraction (50 pixels) was performed using the built-in FIJI plugin. For each channel and ROI, the area, intensity mean, and intensity SD were computed. Pearson's pairwise correlation between channels was performed pixel-wise using a custom-built implementation with no thresholding. This was computed independently for each ROI by creating new images with the mean intensity subtracted, normalized by the SD, and multiplying across both channels:

$$CorrImg_{ROI} = \frac{Img_{ROI,Ch1} - Mean(Img_{ROI,Ch1})}{SD(Img_{ROI,Ch1})} \times \frac{Img_{ROI,Ch2} - Mean(Img_{ROI,Ch2})}{SD(Img_{ROI,Ch2})}$$

This resulting correlation image was then averaged over the extent of the ROI to compute the Pearson's correlation between the two channels for each ROI.

Cells were manually counted for colocalization analysis with the built-in FIJI multiselect tool independently for each channel in 3-4 sections for each subject. The above macro was used to subdivide the counts between ROIs, compute the average cell intensity, ROI intensity, and ROI area. For *Pvalb-Oprm1* ISH colocalization, the average signal-to-noise ratio (SNR), defined as the mean cell intensity divided by the mean ROI SD, across all ROIs and subjects was $SNR_{Pvalb}$ = 9.7 ± 1.0, $SNR_{Oprm1}$ = 9.9 ± 2.1, both of which were significantly greater than 1 ($SNR_{Pvalb}$: $p = 0.0033$, $SNR_{Oprm1}$: $p = 0.0251$, Table S1). For PV-Tac1 IHC colocalization, across all ROIs and subjects, $SNR_{PV}$ = 3.92 ± 0.37, $SNR_{Tac1}$ = 6.27 ± 0.28, both of which were significantly greater than 1 ($SNR_{PV}$: $p = 0.0005$, $SNR_{Tac1}$: $p < 0.0001$, Table S5). For SST-Tac1 IHC colocalization, across all ROIs and subjects, $SNR_{SST}$ = 9.52 ± 1.08, $SNR_{Tac1}$ = 5.83 ± 0.70, both of which were significantly greater than 1 ($SNR_{SST}$: $p < 0.0001$, $SNR_{Tac1}$: $p < 0.0001$, Table S5). Cell counts were summed across all sections for a given subject and ROI.

***RiboTag***

This assay was performed as previously described[48-50]. RNA bound with anti-HA immunoprecipitates and RNA from bulk tissue were purified using RNeasy Plus Micro Kit (Qiagen, Cat# 74034) and the quality of RNA was measured using RNA 6000 Pico kit (Agilent, Cat# 5067-1513) and 2100 Bioanalyzer system (Agilent, Cat# G2939BA). cDNA libraries were constructed from 250 pg RNA using the SMARTer Stranded Total RNA-Seq. Kit v2 (Takara Bio, Cat# 634411) from samples with RNA Integrity Numbers > 6. Sequencing of the libraries were performed on the Illumina HiSeq 2500, at 50 million 2 × 100 bp paired-end reads per sample. ~75% of reads were uniquely mapped to genomic features in the reference genome. Bioconductor package DESeq2[102] was used to identify differentially expressed genes (DEG). This package allows for statistical determination of DEGs using a negative binomial distribution model. The resulting values were then adjusted using the Benjamini and Hochberg's method for controlling the false discovery rate.

***Morphine Injections***

$PV^{Cre/+}$:$ChR2^{fl/+}$ mice were injected subcutaneously with morphine or saline in three treatment regimens, including a bolus injection (15 mg/kg), a chronic treatment with increasing doses over 6 days (15, 20, 25, 30, 40, 50 mg/kg), and a withdrawal group receiving the chronic treatment but with delayed acute slice preparation. Morphine Sulfate (4 mg/mL, Hikma Pharmaceuticals, NDC:0641-6125) was diluted in saline so that each mouse received the same total volume (300 mL). Injections were performed at 9 AM each day, with acute slices prepared one hour after the final injection, except for the withdrawal

group in which 72 hours passed. Mice were injected on a staggered alternating schedule so that 1 mouse was recorded from each day, alternating between saline and morphine.

### *QUANTIFICATION AND STATISTICAL ANALYSIS*

Statistical analysis was conducted in Graphpad Prism 10. All data were tested for normality and lognormality with Shapiro-Wilk tests. Parametric tests were selected if all groups were normal. If at least one group was non-normal and all groups were log-normal, data were log-transformed prior to parametric testing. If data were neither normal nor log-normal, non-parametric tests were used whenever available. Throughout, summary data are presented as mean ± SEM with symbols representing individual values. Additional descriptive statistics and details of hypotheses testing are available for each figure in an accompanying table (see Supplemental Information).

Cellular responses to drug treatments were analyzed with a 1-way repeated-measures design (ANOVA/Friedman, with Tukey's/Dunn's *post hoc* multiple comparisons). All statistical tests were conducted on raw non-normalized data, including plots showing responses normalized to baseline. Experiments missing at most one condition (CTAP/naltrindole) were included and analyzed with a mixed-effects model. Comparisons of the normalized DAMGO responses between regions were performed with a 1-sample t-test/Wilcoxon, comparing to 1 (baseline) and correcting sigma for the number of comparisons. Comparisons between different brain regions' drug responses over time were analyzed with a 2-way design (region × time), with Šídák's multiple comparisons restricted to comparisons between time-equivalent bins. In general, *post hoc* tests for 2-way analyses were restricted to comparisons of *a priori* interest, employing Šídák's or Fisher's multiple comparisons tests.

## SUPPLEMENTAL INFORMATION

***Fig. S2: Layer and sex effects of IeIPSCs.***

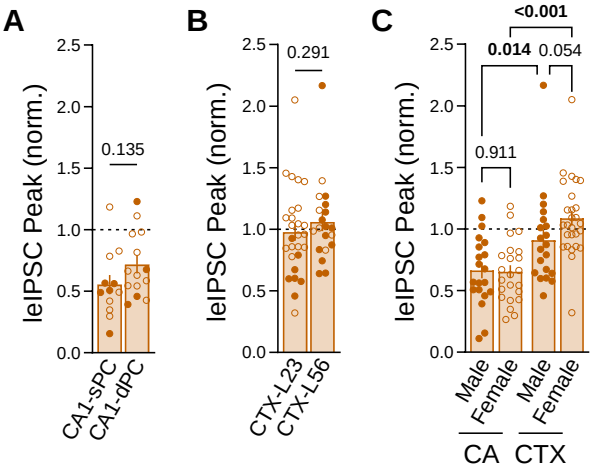


Normalized IeIPSC responses to bath administration of 100 nM DAMGO compared between (**A**) superficial ($n_{sPC}$ = 12) and deep CA1-PCs ($n_{dPC}$ = 14) (**B**) supragranular L2/3 ($n_{L23PC}$ = 27) and infragranular L5/6 neocortical PCs ($n_{L56PC}$ = 30), and (**C**) sex effects across CA-PCs ($n_{malePC}$ = 20, $n_{femalePC}$ = 23) and CTX-PCs ($n_{malePC}$ = 20, $n_{femalePC}$ = 27). P-values indicated in brackets above comparisons. See Table S2 for statistical details.

***Fig. S4: Macaque S5E2-IN consistent with murine PV-IN synaptic transmission.***

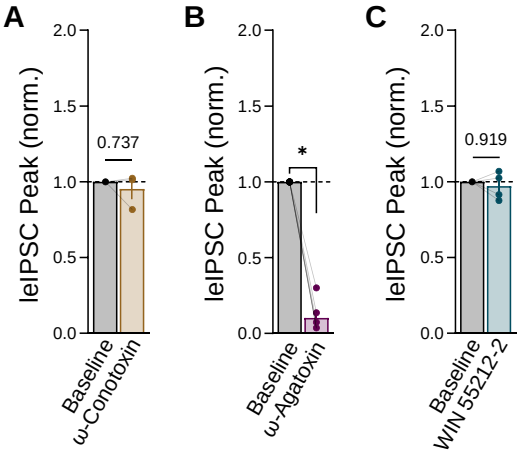


Normalized IeIPSC responses to bath administration of (**A**) 500 nM ω-conotoxin in $n_{cell}$ = 3 CA-PCs, (**B**) 250 nM ω-agatoxin in $n_{cell}$ = 6 CA-PCs, and (**C**) 5 μM WIN 55212-2 in $n_{cell}$ =4 CA-PCs. All experiments performed in 1M macaque, age = 15.9 years. Comparison values indicate non-significant p-values, * $p < 0.05$. See Table S4 for statistical details.

***Table S1: Statistical details for Fig. 1***

***Table S2: Statistical details for Fig. 2 and Fig. S2***

***Table S3: Statistical details for Fig. 3***

***Table S4: Statistical details for Fig. 4 and Fig. S4***

***Table S5: Statistical details for Fig. 5***

***Table S6: Statistical details for Fig. 6***

## REFERENCES


1. Le Merrer, J., Becker, J.A., Befort, K., and Kieffer, B.L. (2009). Reward processing by the opioid system in the brain. Physiol Rev *89*, 1379-1412. 10.1152/physrev.00005.2009.

2. Corder, G., Castro, D.C., Bruchas, M.R., and Scherrer, G. (2018). Endogenous and Exogenous Opioids in Pain. Annu Rev Neurosci *41*, 453-473. 10.1146/annurev-neuro-080317-061522.

3. Spencer, M.R., Miniño, A.M., and Warner, M. (2022). Drug Overdose Deaths in the United States, 2001-2021. NCHS Data Brief, 1-8.

4. Florence, C., Luo, F., and Rice, K. (2021). The economic burden of opioid use disorder and fatal opioid overdose in the United States, 2017. Drug Alcohol Depend *218*, 108350. 10.1016/j.drugalcdep.2020.108350.

5. St Marie, B., Coleman, L., Vignato, J.A., Arndt, S., and Segre, L.S. (2020). Use and Misuse of Opioid Pain Medications by Pregnant and Nonpregnant Women. Pain Manag Nurs *21*, 90-93. 10.1016/j.pmn.2019.05.002.

6. Lee, S.J., Bora, S., Austin, N.C., Westerman, A., and Henderson, J.M.T. (2020). Neurodevelopmental Outcomes of Children Born to Opioid-Dependent Mothers: A Systematic Review and Meta-Analysis. Acad Pediatr *20*, 308-318. 10.1016/j.acap.2019.11.005.

7. Nummenmaa, L., Saanijoki, T., Tuominen, L., Hirvonen, J., Tuulari, J.J., Nuutila, P., and Kalliokoski, K. (2018). μ-opioid receptor system mediates reward processing in humans. Nat Commun *9*, 1500. 10.1038/s41467-018-03848-y.

8. Contet, C., Kieffer, B.L., and Befort, K. (2004). Mu opioid receptor: a gateway to drug addiction. Curr Opin Neurobiol *14*, 370-378. 10.1016/j.conb.2004.05.005.

9. Al-Hasani, R., and Bruchas, M.R. (2011). Molecular mechanisms of opioid receptor-dependent signaling and behavior. Anesthesiology *115*, 1363-1381. 10.1097/ALN.0b013e318238bba6.

10. Valentino, R.J., and Volkow, N.D. (2018). Untangling the complexity of opioid receptor function. Neuropsychopharmacology *43*, 2514-2520. 10.1038/s41386-018-0225-3.

11. Bourinet, E., Soong, T.W., Stea, A., and Snutch, T.P. (1996). Determinants of the G protein-dependent opioid modulation of neuronal calcium channels. Proc Natl Acad Sci U S A *93*, 1486-1491. 10.1073/pnas.93.4.1486.

12. Rusin, K.I., Giovannucci, D.R., Stuenkel, E.L., and Moises, H.C. (1997). Kappa-opioid receptor activation modulates Ca2+ currents and secretion in isolated neuroendocrine nerve terminals. J Neurosci *17*, 6565-6574. 10.1523/jneurosci.17-17-06565.1997.

13. Svoboda, K.R., and Lupica, C.R. (1998). Opioid inhibition of hippocampal interneurons via modulation of potassium and hyperpolarization-activated cation (Ih) currents. J Neurosci *18*, 7084-7098. 10.1523/jneurosci.18-18-07084.1998.

14. Torrecilla, M., Marker, C.L., Cintora, S.C., Stoffel, M., Williams, J.T., and Wickman, K. (2002). G-protein-gated potassium channels containing Kir3.2 and Kir3.3 subunits mediate the acute inhibitory effects of opioids on locus ceruleus neurons. J Neurosci *22*, 4328-4334. 10.1523/jneurosci.22-11-04328.2002.

15. Torrecilla, M., Quillinan, N., Williams, J.T., and Wickman, K. (2008). Pre- and postsynaptic regulation of locus coeruleus neurons after chronic morphine treatment: a study of GIRK-knockout mice. Eur J Neurosci *28*, 618-624. 10.1111/j.1460-9568.2008.06348.x.

16. Ingram, S.L., and Williams, J.T. (1994). Opioid inhibition of Ih via adenylyl cyclase. Neuron *13*, 179-186. 10.1016/0896-6273(94)90468-5.

17. Wimpey, T.L., and Chavkin, C. (1991). Opioids activate both an inward rectifier and a novel voltage-gated potassium conductance in the hippocampal formation. Neuron *6*, 281-289. 10.1016/0896-6273(91)90363-5.

18. Nicoll, R.A., Siggins, G.R., Ling, N., Bloom, F.E., and Guillemin, R. (1977). Neuronal actions of endorphins and enkephalins among brain regions: a comparative microiontophoretic study. Proc Natl Acad Sci U S A *74*, 2584-2588. 10.1073/pnas.74.6.2584.

19. Lupica, C.R., Proctor, W.R., and Dunwiddie, T.V. (1992). Dissociation of mu and delta opioid receptor-mediated reductions in evoked and spontaneous synaptic inhibition in the rat hippocampus in vitro. Brain Res *593*, 226-238. 10.1016/0006-8993(92)91312-3.

20. Capogna, M., Gähwiler, B.H., and Thompson, S.M. (1993). Mechanism of mu-opioid receptor-mediated presynaptic inhibition in the rat hippocampus in vitro. J Physiol *470*, 539-558. 10.1113/jphysiol.1993.sp019874.

21. Lupica, C.R. (1995). Delta and mu enkephalins inhibit spontaneous GABA-mediated IPSCs via a cyclic AMP-independent mechanism in the rat hippocampus. J Neurosci *15*, 737-749. 10.1523/jneurosci.15-01-00737.1995.

22. Zieglgänsberger, W., French, E.D., Siggins, G.R., and Bloom, F.E. (1979). Opioid peptides may excite hippocampal pyramidal neurons by inhibiting adjacent inhibitory interneurons. Science *205*, 415-417. 10.1126/science.451610.

23. Nicoll, R.A., Alger, B.E., and Jahr, C.E. (1980). Enkephalin blocks inhibitory pathways in the vertebrate CNS. Nature *287*, 22-25. 10.1038/287022a0.

24. Madison, D.V., and Nicoll, R.A. (1988). Enkephalin hyperpolarizes interneurones in the rat hippocampus. J Physiol *398*, 123-130. 10.1113/jphysiol.1988.sp017033.

25. Glickfeld, L.L., Atallah, B.V., and Scanziani, M. (2008). Complementary modulation of somatic inhibition by opioids and cannabinoids. J Neurosci *28*, 1824-1832. 10.1523/jneurosci.4700-07.2008.

26. Shao, C., Chen, P., Chen, Q., Zhao, M., Zhang, W.N., and Yang, K. (2020). Mu opioid receptors inhibit GABA release from parvalbumin interneuron terminals onto CA1 pyramidal cells. Biochem Biophys Res Commun *522*, 1059-1062. 10.1016/j.bbrc.2019.12.013.

27. He, X.J., Patel, J., Weiss, C.E., Ma, X., Bloodgood, B.L., and Banghart, M.R. (2021). Convergent, functionally independent signaling by mu and delta opioid receptors in hippocampal parvalbumin interneurons. Elife *10*. 10.7554/eLife.69746.

28. Drake, C.T., and Milner, T.A. (2002). Mu opioid receptors are in discrete hippocampal interneuron subpopulations. Hippocampus *12*, 119-136. 10.1002/hipo.1107.

29. Stumm, R.K., Zhou, C., Schulz, S., and Höllt, V. (2004). Neuronal types expressing mu- and delta-opioid receptor mRNA in the rat hippocampal formation. J Comp Neurol *469*, 107-118. 10.1002/cne.10997.

30. Svoboda, K.R., Adams, C.E., and Lupica, C.R. (1999). Opioid receptor subtype expression defines morphologically distinct classes of hippocampal interneurons. J Neurosci *19*, 85-95. 10.1523/jneurosci.19-01-00085.1999.

31. Krook-Magnuson, E., Luu, L., Lee, S.H., Varga, C., and Soltesz, I. (2011). Ivy and neurogliaform interneurons are a major target of μ-opioid receptor modulation. J Neurosci *31*, 14861-14870. 10.1523/jneurosci.2269-11.2011.

32. George, S.R., Zastawny, R.L., Briones-Urbina, R., Cheng, R., Nguyen, T., Heiber, M., Kouvelas, A., Chan, A.S., and O'Dowd, B.F. (1994). Distinct distributions of mu, delta and kappa opioid receptor mRNA in rat brain. Biochem Biophys Res Commun *205*, 1438-1444. 10.1006/bbrc.1994.2826.

33. Mansour, A., Fox, C.A., Burke, S., Meng, F., Thompson, R.C., Akil, H., and Watson, S.J. (1994). Mu, delta, and kappa opioid receptor mRNA expression in the rat CNS: an in situ hybridization study. J Comp Neurol *350*, 412-438. 10.1002/cne.903500307.

34. Cahill, C.M., McClellan, K.A., Morinville, A., Hoffert, C., Hubatsch, D., O'Donnell, D., and Beaudet, A. (2001). Immunohistochemical distribution of delta opioid receptors in the rat central nervous system: evidence for somatodendritic labeling and antigen-specific cellular compartmentalization. J Comp Neurol *440*, 65-84. 10.1002/cne.1370.

35. Erbs, E., Faget, L., Scherrer, G., Matifas, A., Filliol, D., Vonesch, J.L., Koch, M., Kessler, P., Hentsch, D., Birling, M.C., et al. (2015). A mu-delta opioid receptor brain atlas reveals neuronal co-occurrence in subcortical networks. Brain Struct Funct *220*, 677-702. 10.1007/s00429-014-0717-9.

36. Ehrlich, A.T., Semache, M., Gross, F., Da Fonte, D.F., Runtz, L., Colley, C., Mezni, A., Le Gouill, C., Lukasheva, V., Hogue, M., et al. (2019). Biased Signaling of the Mu Opioid Receptor Revealed in Native Neurons. iScience *14*, 47-57. 10.1016/j.isci.2019.03.011.

37. Hu, H., Gan, J., and Jonas, P. (2014). Fast-spiking, parvalbumin+ GABAergic interneurons: From cellular design to microcircuit function. Science *345*, 1255263. 10.1126/science.1255263.

38. Wonders, C.P., and Anderson, S.A. (2006). The origin and specification of cortical interneurons. Nat Rev Neurosci *7*, 687-696. 10.1038/nrn1954.

39. Armstrong, C., and Soltesz, I. (2012). Basket cell dichotomy in microcircuit function. J Physiol *590*, 683-694. 10.1113/jphysiol.2011.223669.

40. Uchigashima, M., Narushima, M., Fukaya, M., Katona, I., Kano, M., and Watanabe, M. (2007). Subcellular arrangement of molecules for 2-arachidonoyl-glycerol-mediated retrograde signaling and its physiological contribution to synaptic modulation in the striatum. J Neurosci *27*, 3663-3676. 10.1523/jneurosci.0448-07.2007.

41. Wilson, R.I., and Nicoll, R.A. (2002). Endocannabinoid signaling in the brain. Science *296*, 678-682. 10.1126/science.1063545.

42. Lee, B.R., Dalley, R., Miller, J.A., Chartrand, T., Close, J., Mann, R., Mukora, A., Ng, L., Alfiler, L., Baker, K., et al. (2023). Signature morphoelectric properties of diverse GABAergic interneurons in the human neocortex. Science *382*, eadf6484. 10.1126/science.adf6484.

43. Szegedi, V., Bakos, E., Furdan, S., Kovács, B.H., Varga, D., Erdélyi, M., Barzó, P., Szücs, A., Tamás, G., and Lamsa, K. (2023). HCN channels at the cell soma ensure the rapid electrical reactivity of fast-spiking interneurons in human neocortex. PLoS Biol *21*, e3002001. 10.1371/journal.pbio.3002001.

44. Vormstein-Schneider, D., Lin, J.D., Pelkey, K.A., Chittajallu, R., Guo, B., Arias-Garcia, M.A., Allaway, K., Sakopoulos, S., Schneider, G., Stevenson, O., et al. (2020). Viral manipulation of functionally distinct interneurons in mice, non-human primates and humans. Nature Neuroscience. 10.1038/s41593-020-0692-9.

45. Giannopoulos, P., and Papatheodoropoulos, C. (2013). Effects of μ-opioid receptor modulation on the hippocampal network activity of sharp wave and ripples. British Journal of Pharmacology *168*, 1146-1164. 10.1111/j.1476-5381.2012.02240.x.

46. Gulyás, A.I., Szabó, G.G., Ulbert, I., Holderith, N., Monyer, H., Erdélyi, F., Szabó, G., Freund, T.F., and Hájos, N. (2010). Parvalbumin-Containing Fast-Spiking Basket Cells Generate the Field Potential Oscillations Induced by Cholinergic Receptor Activation in the Hippocampus. Journal of Neuroscience *30*, 15134-15145. 10.1523/JNEUROSCI.4104-10.2010.

47. Tricoire, L., Pelkey, K.A., Erkkila, B.E., Jeffries, B.W., Yuan, X., and McBain, C.J. (2011). A blueprint for the spatiotemporal origins of mouse hippocampal interneuron diversity. The Journal of Neuroscience: The Official Journal of the Society for Neuroscience *31*, 10948-10970. 10.1523/JNEUROSCI.0323-11.2011.

48. Sanz, E., Yang, L., Su, T., Morris, D.R., McKnight, G.S., and Amieux, P.S. (2009). Cell-type-specific isolation of ribosome-associated mRNA from complex tissues. Proc Natl Acad Sci U S A *106*, 13939-13944. 10.1073/pnas.0907143106.

49. Mahadevan, V., Peltekian, A., and McBain, C.J. (2020). Translatome Analyses Using Conditional Ribosomal Tagging in GABAergic Interneurons and Other Sparse Cell Types. Current Protocols in Neuroscience *92*, e93. 10.1002/cpns.93.

50. Mahadevan, V., Mitra, A., Zhang, Y., Yuan, X., Peltekian, A., Chittajallu, R., Esnault, C., Maric, D., Rhodes, C., Pelkey, K.A., et al. (2021). NMDARs Drive the Expression of Neuropsychiatric Disorder Risk Genes Within GABAergic Interneuron Subtypes in the Juvenile Brain. Front Mol Neurosci *14*, 712609. 10.3389/fnmol.2021.712609.

51. Lee, S.-H., Marchionni, I., Bezaire, M., Varga, C., Danielson, N., Lovett-Barron, M., Losonczy, A., and Soltesz, I. (2014). Parvalbumin-Positive Basket Cells Differentiate Among Hippocampal Pyramidal Cells. Neuron *82*, 1129-1144. 10.1016/j.neuron.2014.03.034.

52. Valero, M., Cid, E., Averkin, R.G., Aguilar, J., Sanchez-Aguilera, A., Viney, T.J., Gomez-Dominguez, D., Bellistri, E., and Menéndez de la Prida, L. (2015). Determinants of different deep and superficial CA1 pyramidal cell dynamics during sharp-wave ripples. Nature Neuroscience *18*, 1281-1290. 10.1038/nn.4074.

53. Piskorowski, R.A., and Chevaleyre, V. (2013). Delta-opioid receptors mediate unique plasticity onto parvalbumin-expressing interneurons in area CA2 of the hippocampus. J Neurosci *33*, 14567-14578. 10.1523/jneurosci.0649-13.2013.

54. Loyd, D.R., and Murphy, A.Z. (2014). The neuroanatomy of sexual dimorphism in opioid analgesia. Exp Neurol *259*, 57-63. 10.1016/j.expneurol.2014.04.004.

55. Torres-Reveron, A., Williams, T.J., Chapleau, J.D., Waters, E.M., McEwen, B.S., Drake, C.T., and Milner, T.A. (2009). Ovarian steroids alter mu opioid receptor trafficking in hippocampal parvalbumin GABAergic interneurons. Exp Neurol *219*, 319-327. 10.1016/j.expneurol.2009.06.001.

56. Milner, T.A., Burstein, S.R., Marrone, G.F., Khalid, S., Gonzalez, A.D., Williams, T.J., Schierberl, K.C., Torres-Reveron, A., Gonzales, K.L., McEwen, B.S., and Waters, E.M. (2013). Stress differentially alters mu opioid receptor density and trafficking in parvalbumin-containing interneurons in the female and male rat hippocampus. Synapse *67*, 757-772. 10.1002/syn.21683.

57. Berg, J., Sorensen, S.A., Ting, J.T., Miller, J.A., Chartrand, T., Buchin, A., Bakken, T.E., Budzillo, A., Dee, N., Ding, S.L., et al. (2021). Human neocortical expansion involves glutamatergic neuron diversification. Nature *598*, 151-158. 10.1038/s41586-021-03813-8.

58. Kalmbach, B.E., Hodge, R.D., Jorstad, N.L., Owen, S., de Frates, R., Yanny, A.M., Dalley, R., Mallory, M., Graybuck, L.T., Radaelli, C., et al. (2021). Signature morpho-electric, transcriptomic, and dendritic properties of human layer 5 neocortical pyramidal neurons. Neuron *109*, 2914-2927.e2915. 10.1016/j.neuron.2021.08.030.

59. Wilson, R.I., Kunos, G., and Nicoll, R.A. (2001). Presynaptic specificity of endocannabinoid signaling in the hippocampus. Neuron *31*, 453-462. 10.1016/s0896-6273(01)00372-5.

60. Hefft, S., and Jonas, P. (2005). Asynchronous GABA release generates long-lasting inhibition at a hippocampal interneuron-principal neuron synapse. Nat Neurosci *8*, 1319-1328. 10.1038/nn1542.

61. Wilson, R.I., and Nicoll, R.A. (2001). Endogenous cannabinoids mediate retrograde signalling at hippocampal synapses. Nature *410*, 588-592. 10.1038/35069076.

62. Alcántara, S., Ferrer, I., and Soriano, E. (1993). Postnatal development of parvalbumin and calbindin D28K immunoreactivities in the cerebral cortex of the rat. Anat Embryol (Berl) *188*, 63-73. 10.1007/bf00191452.

63. Favuzzi, E., Deogracias, R., Marques-Smith, A., Maeso, P., Jezequel, J., Exposito-Alonso, D., Balia, M., Kroon, T., Hinojosa, A.J., E, F.M., and Rico, B. (2019). Distinct molecular programs regulate synapse specificity in cortical inhibitory circuits. Science *363*, 413-417. 10.1126/science.aau8977.

64. Camp, C.R., Vlachos, A., Klöckner, C., Krey, I., Banke, T.G., Shariatzadeh, N., Ruggiero, S.M., Galer, P., Park, K.L., Caccavano, A., et al. (2023). Loss of Grin2a causes a transient delay in the electrophysiological maturation of hippocampal parvalbumin interneurons. Commun Biol *6*, 952. 10.1038/s42003-023-05298-9.

65. Chamberland, S., Grant, G., Machold, R., Nebet, E.R., Tian, G., Hanani, M., Kullander, K., and Tsien, R.W. (2023). Functional specialization of hippocampal somatostatin-expressing interneurons. bioRxiv. 10.1101/2023.04.27.538511.

66. Ben-Ari, Y., Cherubini, E., Corradetti, R., and Gaiarsa, J.L. (1989). Giant synaptic potentials in immature rat CA3 hippocampal neurones. J Physiol *416*, 303-325. 10.1113/jphysiol.1989.sp017762.

67. Ben-Ari, Y. (2001). Developing networks play a similar melody. Trends Neurosci *24*, 353-360. 10.1016/s0166-2236(00)01813-0.

68. Wester, J.C., and McBain, C.J. (2016). Interneurons Differentially Contribute to Spontaneous Network Activity in the Developing Hippocampus Dependent on Their Embryonic Lineage. J Neurosci *36*, 2646-2662. 10.1523/jneurosci.4000-15.2016.

69. Bonifazi, P., Goldin, M., Picardo, M.A., Jorquera, I., Cattani, A., Bianconi, G., Represa, A., Ben-Ari, Y., and Cossart, R. (2009). GABAergic hub neurons orchestrate synchrony in developing hippocampal networks. Science *326*, 1419-1424. 10.1126/science.1175509.

70. Picardo, M.A., Guigue, P., Bonifazi, P., Batista-Brito, R., Allene, C., Ribas, A., Fishell, G., Baude, A., and Cossart, R. (2011). Pioneer GABA cells comprise a subpopulation of hub neurons in the developing hippocampus. Neuron *71*, 695-709. 10.1016/j.neuron.2011.06.018.

71. Flossmann, T., Kaas, T., Rahmati, V., Kiebel, S.J., Witte, O.W., Holthoff, K., and Kirmse, K. (2019). Somatostatin Interneurons Promote Neuronal Synchrony in the Neonatal Hippocampus. Cell Rep *26*, 3173-3182.e3175. 10.1016/j.celrep.2019.02.061.

72. Wang, Z., Bilsky, E.J., Porreca, F., and Sadée, W. (1994). Constitutive mu opioid receptor activation as a regulatory mechanism underlying narcotic tolerance and dependence. Life Sci *54*, Pl339-350. 10.1016/0024-3205(94)90022-1.

73. Neilan, C.L., Akil, H., Woods, J.H., and Traynor, J.R. (1999). Constitutive activity of the delta-opioid receptor expressed in C6 glioma cells: identification of non-peptide delta-inverse agonists. Br J Pharmacol *128*, 556-562. 10.1038/sj.bjp.0702816.

74. Liu, J.G., and Prather, P.L. (2001). Chronic exposure to mu-opioid agonists produces constitutive activation of mu-opioid receptors in direct proportion to the efficacy of the agonist used for pretreatment. Mol Pharmacol *60*, 53-62. 10.1124/mol.60.1.53.

75. Shoblock, J.R., and Maidment, N.T. (2006). Constitutively active micro opioid receptors mediate the enhanced conditioned aversive effect of naloxone in morphine-dependent mice. Neuropsychopharmacology *31*, 171-177. 10.1038/sj.npp.1300782.

76. Meye, F.J., van Zessen, R., Smidt, M.P., Adan, R.A., and Ramakers, G.M. (2012). Morphine withdrawal enhances constitutive μ-opioid receptor activity in the ventral tegmental area. J Neurosci *32*, 16120-16128. 10.1523/jneurosci.1572-12.2012.

77. Basheer, R., and Tempel, A. (1993). Morphine-induced reciprocal alterations in G alpha s and opioid peptide mRNA levels in discrete brain regions. J Neurosci Res *36*, 551-557. 10.1002/jnr.490360507.

78. Taki, K., Kaneko, T., and Mizuno, N. (2000). A group of cortical interneurons expressing μ-opioid receptor-like immunoreactivity: a double immunofluorescence study in the rat cerebral cortex. Neuroscience *98*, 221-231. 10.1016/s0306-4522(00)00124-x.

79. Blasco-Ibáñez, J.M., Martínez-Guijarro, F.J., and Freund, T.F. (1998). Enkephalin-containing interneurons are specialized to innervate other interneurons in the hippocampal CA1 region of the rat and guinea-pig. Eur J Neurosci *10*, 1784-1795. 10.1046/j.1460-9568.1998.00190.x.

80. Leroy, F., de Solis, C.A., Boyle, L.M., Bock, T., Lofaro, O.M., Buss, E.W., Asok, A., Kandel, E.R., and Siegelbaum, S.A. (2021). Enkephalin release from VIP interneurons in the hippocampal CA2/3a region mediates heterosynaptic plasticity and social memory. Mol Psychiatry. 10.1038/s41380-021-01124-y.

81. Gurgenidze, S., Bäuerle, P., Schmitz, D., Vida, I., Gloveli, T., and Dugladze, T. (2022). Cell-Type Specific Inhibition Controls the High-Frequency Oscillations in the Medial Entorhinal Cortex. Int J Mol Sci *23*. 10.3390/ijms232214087.

82. Lau, B.K., Ambrose, B.P., Thomas, C.S., Qiao, M., and Borgland, S.L. (2020). Mu-Opioids Suppress GABAergic Synaptic Transmission onto Orbitofrontal Cortex Pyramidal Neurons with Subregional Selectivity. J Neurosci *40*, 5894-5907. 10.1523/jneurosci.2049-19.2020.

83. Jiang, C., Wang, X., Le, Q., Liu, P., Liu, C., Wang, Z., He, G., Zheng, P., Wang, F., and Ma, L. (2021). Morphine coordinates SST and PV interneurons in the prelimbic cortex to disinhibit pyramidal neurons and enhance reward. Mol Psychiatry *26*, 1178-1193. 10.1038/s41380-019-0480-7.

84. Preuss, T.M., and Wise, S.P. (2022). Evolution of prefrontal cortex. Neuropsychopharmacology *47*, 3-19. 10.1038/s41386-021-01076-5.

85. Miyoshi, G., Butt, S.J., Takebayashi, H., and Fishell, G. (2007). Physiologically distinct temporal cohorts of cortical interneurons arise from telencephalic Olig2-expressing precursors. J Neurosci *27*, 7786-7798. 10.1523/jneurosci.1807-07.2007.

86. Butt, S.J., Fuccillo, M., Nery, S., Noctor, S., Kriegstein, A., Corbin, J.G., and Fishell, G. (2005). The temporal and spatial origins of cortical interneurons predict their physiological subtype. Neuron *48*, 591-604. 10.1016/j.neuron.2005.09.034.

87. Donato, F., Chowdhury, A., Lahr, M., and Caroni, P. (2015). Early- and late-born parvalbumin basket cell subpopulations exhibiting distinct regulation and roles in learning. Neuron *85*, 770-786. 10.1016/j.neuron.2015.01.011.

88. Cossart, R., and Khazipov, R. (2021). How development sculpts hippocampal circuits and function. Physiol Rev. 10.1152/physrev.00044.2020.

89. Xie, C.W., and Lewis, D.V. (1991). Opioid-mediated facilitation of long-term potentiation at the lateral perforant path-dentate granule cell synapse. J Pharmacol Exp Ther *256*, 289-296.

90. Bramham, C.R., and Sarvey, J.M. (1996). Endogenous activation of mu and delta-1 opioid receptors is required for long-term potentiation induction in the lateral perforant path: dependence on GABAergic inhibition. J Neurosci *16*, 8123-8131. 10.1523/jneurosci.16-24-08123.1996.

91. Mansouri, F.A., Motamedi, F., Fathollahi, Y., Atapour, N., and Semnanian, S. (1997). Augmentation of LTP induced by primed-bursts tetanic stimulation in hippocampal CA1 area of morphine dependent rats. Brain Res *769*, 119-124. 10.1016/s0006-8993(97)00608-2.

92. Pu, L., Bao, G.B., Xu, N.J., Ma, L., and Pei, G. (2002). Hippocampal long-term potentiation is reduced by chronic opiate treatment and can be restored by re-exposure to opiates. J Neurosci *22*, 1914-1921. 10.1523/jneurosci.22-05-01914.2002.

93. McQuiston, A.R. (2008). Layer selective presynaptic modulation of excitatory inputs to hippocampal cornu Ammon 1 by mu-opioid receptor activation. Neuroscience *151*, 209-221. 10.1016/j.neuroscience.2007.09.077.

94. Valero, M., Navas-Olive, A., de la Prida, L.M., and Buzsáki, G. (2022). Inhibitory conductance controls place field dynamics in the hippocampus. Cell Rep *40*, 111232. 10.1016/j.celrep.2022.111232.

95. Hippenmeyer, S., Vrieseling, E., Sigrist, M., Portmann, T., Laengle, C., Ladle, D.R., and Arber, S. (2005). A developmental switch in the response of DRG neurons to ETS transcription factor signaling. PLoS biology *3*, e159. 10.1371/journal.pbio.0030159.

96. Taniguchi, H., He, M., Wu, P., Kim, S., Paik, R., Sugino, K., Kvitsiani, D., Kvitsani, D., Fu, Y., Lu, J., et al. (2011). A resource of Cre driver lines for genetic targeting of GABAergic neurons in cerebral cortex. Neuron *71*, 995-1013. 10.1016/j.neuron.2011.07.026.

97. Harris, J.A., Hirokawa, K.E., Sorensen, S.A., Gu, H., Mills, M., Ng, L.L., Bohn, P., Mortrud, M., Ouellette, B., Kidney, J., et al. (2014). Anatomical characterization of Cre driver mice for neural circuit mapping and manipulation. Front Neural Circuits *8*, 76. 10.3389/fncir.2014.00076.

98. Xu, Q., Tam, M., and Anderson, S.A. (2008). Fate mapping Nkx2.1-lineage cells in the mouse telencephalon. J Comp Neurol *506*, 16-29. 10.1002/cne.21529.

99. Madisen, L., Zwingman, T.A., Sunkin, S.M., Oh, S.W., Zariwala, H.A., Gu, H., Ng, L.L., Palmiter, R.D., Hawrylycz, M.J., Jones, A.R., et al. (2010). A robust and high-throughput Cre reporting and characterization system for the whole mouse brain. Nature Neuroscience *13*, 133-140. 10.1038/nn.2467.

100. Madisen, L., Mao, T., Koch, H., Zhuo, J.M., Berenyi, A., Fujisawa, S., Hsu, Y.W., Garcia, A.J., 3rd, Gu, X., Zanella, S., et al. (2012). A toolbox of Cre-dependent optogenetic transgenic mice for light-induced activation and silencing. Nat Neurosci *15*, 793-802. 10.1038/nn.3078.

101. Daigle, T.L., Madisen, L., Hage, T.A., Valley, M.T., Knoblich, U., Larsen, R.S., Takeno, M.M., Huang, L., Gu, H., Larsen, R., et al. (2018). A Suite of Transgenic Driver and Reporter Mouse Lines with Enhanced Brain-Cell-Type Targeting and Functionality. Cell *174*, 465-480.e422. 10.1016/j.cell.2018.06.035.

102. Love, M.I., Huber, W., and Anders, S. (2014). Moderated estimation of fold change and dispersion for RNA-seq data with DESeq2. Genome Biol *15*, 550. 10.1186/s13059-014-0550-8.

103. Fredericks, J.M., Dash, K.E., Jaskot, E.M., Bennett, T.W., Lerchner, W., Dold, G., Ide, D., Cummins, A.C., Der Minassian, V.H., Turchi, J.N., et al. (2020). Methods for mechanical delivery of viral vectors into rhesus monkey brain. J Neurosci Methods *339*, 108730. 10.1016/j.jneumeth.2020.108730.